2013

Structural and Conformational Probing of 2-Acetylaminofluorene-Modified -1, -2 and -3 Slipped Mutagenic Intermediates

Anusha Sandineni
University of Rhode Island, asandineni@my.uri.edu

STRUCTURAL AND CONFORMATIONAL PROBING OF 2-ACETYLAMINOFLUORENE-MODIFIED -1, -2 AND -3 SLIPPED MUTAGENIC INTERMEDIATES

BY

ANUSHA SANDINENI

A THESIS SUBMITTED IN PARTIAL FULFILLMENT OF THE

REQUIREMENTS FOR THE DEGREE OF

MASTER OF SCIENCE

IN

BIOMEDICAL AND PHARMACEUTICAL SCIENCES

UNIVERSITY OF RHODE ISLAND

2013

MASTER OF SCIENCE THESIS

OF

Anusha Sandineni

APPROVED:

Thesis Committee:

Major Professor: DR. BONGSUP CHO

DR. ROBERTA KING

DR. ANGELA SLITT

DR. MINDY LEVINE

DR. DEBOEF

DEAN OF THE GRADUATE SCHOOL

NASSER H. ZAWIA

UNIVERSITY OF RHODE ISLAND

2013

ABSTRACT

2-Acetylaminofluorene (AAF) is a prototype arylamine carcinogen that forms C8-substituted dG-adduct (dG-C8-AAF) as a major DNA damage. The bulky dG-C8-AAF lesion is known to induce -1, -2, or -3 frameshift mutations depending on the base sequences around the lesion. We hypothesize that the stability of bulged-out structures slipped mutagenic intermediate (SMI) facilitates primer elongation, hence manifestation of frameshift mutations. The objective of the present study was to probe the structural/conformational basis of various dG-C8-AAF induced frameshift mutations. Here, we describe spectroscopic (^{19}F NMR and CD) and thermodynamic (UV-melting and DSC) studies of several dG-C8-FAAF-modified 16-mer DNA duplexes containing fully-paired, -2, and -3 deletion duplexes on the 5'-CTCTCGATG[FAAF]CCATCAC-3' sequence and -1 deletion duplexes on either the 5'-CTCTCGATG[FAAF]CCATCAC-3' or 5'-CTCTCGGCG [FAAF]CCATCAC-3' sequences. The results were analyzed to determine the conformational and thermodynamic basis of AAF-induced frameshift mutagenesis. We found that the dG-AAF lesion exists in a mixture of external binding B and inserted/bulge conformers and the population of the latter was in order of 'GC'-1(73%) > 'AT' -1 (72%) > full (60%) > -2 (55%) > -3 (37%). Thermodynamic stability was found to be in order of -1 deletion > -2 deletion > fully paired > -3 deletion duplexes. These results indicate that the stacked conformer especially in the deletion duplexes is thermodynamically more stable than the conformationally flexible external B-conformer. Previous primer extension results involving the human DNA polymerase η have shown that the frequency of deletion was in order of -1 > -2 > -3. Taken together, our results

support the hypothesis that the conformational and thermodynamic stability of the SMI is a critical determinant for the induction of various frameshift mutations.

ACKNOWLEDGEMENTS

I would like to thank Dr. Bongsup Cho, my major advisor, for providing me this opportunity to work in his group. He is a great teacher. I took his Drug metabolism and Medicinal chemistry classes which were very interesting. He helped me in improving my presentation skills and always explained me clearly what I need to do when I have any problem in research and related issues. I was inspired by him both professionally and personally, he is an ideal mentor to me. I would also like to thank my Committee members Drs. King, Slitt, Deboef, and Levine for their support.

I also like to thank my colleagues Dr. Patnaik for helping me with the synthesis of AAF carcinogen and HPLC training initially, Vipin Jain for guiding me with my course work and other experimental and technical problems in my research such as NMR experiments, Dr. Ganesan for providing literature which was immensely helpful for writing my Thesis. I would like to thank Lifang Xu for being my friend and giving a good company in most of the classes we had taken together, and helping me with Research and Anshu Jain for helping me with MALDI-TOF experiments. I thank them for their friendships and their helpful discussions.

I would like to thank my uncle Dr. Srinivasa rao Meneni and his family for helping me and taking care of me in US. I thank my dear sister Tanuja Sandineni for being my ideal from my childhood. For sharing my problems and for being a good support when i am feeling low, i thank my dear friend Sushma Bollepally.

Finally, I’m indebted to my dearest parents for their unconditional love and continuous support. They helped me in choosing a right career path. They are always special in my life and I am inspired by them.

PREFACE

This thesis is written in Standard format.

Chapter 1 provides an introduction on aromatic amine-induced carcinogenesis and the work done on them in the past. Here I propose a hypothesis for my Thesis and specific plans and protocols to rationalize and prove the hypothesis.

Chapter 2 describes detailed experimental methods used in the present study.

Chapter 3 describes the results obtained from the proposed work.

Chapter 4 discusses the results in detail in terms of previous literature work and biological implications.

TABLE OF CONTENTS

Page

LIST OF TABLES

Table **Page**

LIST OF FIGURES

Figure **Page**

CHAPTER I

INTRODUCTION

Aromatic amines are a well-known group of mutagens/carcinogens that cause cancer initiation (*1*). These amines are widely present in the environment as byproducts of fossil fuel combustion, tobacco smoke, dyes, and charred meat. 2-Acetylaminofluorene (AAF) was developed originally as a pesticide, but the compound was never used for its intended purpose because of its potent liver carcinogenicity in rodents (*2*). Instead, AAF has become a prototype molecule for investigating the mechanisms of aromatic amine-induced carcinogenesis (*3*). Upon activation in the liver, AAF is converted into a highly electrophilic nitrenium ion, which in turn reacts directly with cellular DNA to form covalent DNA adducts. The most commonly formed are C8-substituted 2'-deoxyguanosine adducts: the N-acetylated dG-C8-AAF, [N-(2′-deoxyguanosin-8-yl)-2-acetylaminofluorene] and the N-deacetylated dG-C8-AF, [N-(2′-deoxyguanosin-8-yl)-2-aminofluorene] (*2, 4*). Although the two adducts are similar in chemical structures, they exhibit different mutagenic and repair properties. For example, dG-C8-AF is largely non-mutagenic and is correctly replicated by high-fidelity polymerases possibly. This may be due to its flexibility to accommodate both syn- and anti-glycosidic conformation. The latter allows to forms the B-type DNA conformation, supporting Watson-crick base pairs at the lesion site (*5*). On the other hand, the bulky N-acetylated dG-C8-AAF lesion exists primarily in the highly distorting syn stacked (S)- or wedge (W)-conformation,

resulting in a strong block of high fidelity polymerase (*6*). Bypass of the AAF-dG lesion leads to frame shift mutations (*3, 7*).

DNA polymerases are the enzymes that catalyze the polymerization of 2´-deoxyribonucleotides into DNA strands. Polymerases use steric and hydrogen-bonding interactions to identify the correct nucleotide for insertion opposite each base in the template strand. Duplication of DNA containing damaged bases is a challenge to DNA polymerases that normally replicate with high speed, high accuracy and high processivity in undamaged templates. When a replicative DNA polymerase encounters a chemically altered base that it is unable to copy, a process called TransLesion Synthesis (TLS) takes place during which the polymerase is transiently replaced by a specialized lesion bypass polymerase. The process by which the polymerase proceeds through the adduct in TLS may be either error-free or error pone. Error-free lesion bypass results in the preferential incorporation of a correct nucleotide opposite the damage, whereas error-prone lesion bypass leads to the preferential incorporation of an incorrect nucleotide opposite the damage (*8*). Consequently, error-free lesion bypass is a mutation-avoiding mechanism, whereas error-prone lesion bypass is a mutation-generating mechanism. For example, human DNA polymerase Pol η belongs to the class of Y-family DNA-polymerases. These low fidelity polymerases have larger active sites that can accommodate bulky DNA adducts allowing them to bypass these lesions during replication. The activity of Pol η is critical in preventing the Xeroderma Pigmentosum (XPV) disease (*9*). Recently it was discovered that Pol η is involved in the *in vivo* bypass of dG-C8-AAF, which occurs by base pairing the lesion correctly with dC (*10*). However, dG-C8-AAF in the E. coli hot

spot *Nar*I sequence (5′-$G_1G_2CG_3CC$-3′) is prone to induce a -1 or -2 frame shift mutation (*11-16*).

A majority of AAF-induced mutations in *E. coli* are frameshift mutations (*17*) including additions and deletions of a single G:C base pair, deletions of two adjacent base pairs, and a few three-base-pair deletions (*12, 17*). Frameshift mutations involve gain or loss of one or more base pairs relative to the original sequence, thereby causing a shift in the genetic reading frame, resulting in loss of the whole information content of the gene (*18*). Frameshift mutations induced by AAF can be best explained by a slippage mechanism. A specific mechanism has been proposed to explain the double-base frameshifts in the *Nar*I sequence in which the 'GC' deletion results from a slipped mutagenic intermediate (SMI) formed during replication shown in Figure 1. In the first step, the correct nucleotide dC is incorporated opposite dG-C8-AAF. Hindering of the replication fork at the modified dG favors a misalignment, thereby causing slippage of the growing primer strand and two bases of the *Nar*I sequence are looped out in the parental strand. Continued extension from the two nucleotide bulge in the template strand, leads to a newly synthesized strand two bases shorter than the template strand (*19*). Similarly, in -1 and -3 deletions polymerase extends the primer with a dC base opposite the lesion, however a substantial fraction of the primer misaligns to pair with the 5'-dG next to the lesion in -1 slippage and two bases further away in -3 slippage (shown in Figure 2 (A) (B) respectively) (*20*).

Using high resolution ^{1}H NMR, O'Handley et al (*21*) reported the presence of about 70% base displaced S-conformer in a AAF-modified fully paired 9-mer duplex in the CG*C sequence context. The Cho group has used ^{19}F NMR spectroscopy to show the

exclusive existence of the S-conformer with a novel cis/trans equilibrium of the acetyl group for a fully paired 12-mer duplex in the TG*A sequence context (*22*). Milhe et al. (*23, 24*) obtained ^{1}H NMR data on the AAF modified -1, -2 deletion duplexes on CG*C context. 70% of the AAF-population was external in the -1 deletion duplex, whereas in the -2 deletion duplex, 80% of the fluorene moiety was inserted in to the bulged double helix. However, the NMR data was difficult to interpret because of the conformational heterogeneity. Similar NMR studies were conducted on -1, -2 deletion duplexes by the N-deacetylated AF (*25, 26*) and *anti*-benzo[a]pyrenediol epoxide (BPDE) (*27, 28*). All these deletion duplexes with the exception of AAF -1 duplex, exist primarily in conformation, in which the carcinogenic moiety is inserted in to the helix (*23*). These modified duplexes showed consistent thermal stabilities (ΔTm= 11-15 ℃) relative to controls, which support well-stacked structures.

Recently, Schorr et al (*20*) studied the AAF-induced frame shift mutation in the *Nar*I sequence (5′-$G_1G_2CG_3$CC-3′) using the low fidelity human polymerase η. They found that AAF can induce -1, -2, or -3 frame-shift mutations depending upon the neighboring bases around the lesion. For example, changing of G_2C to AT (5′-$G_1\underline{G_2C}G_3$CC-3′→ 5′-$G_1\underline{AT}G_3$CC-3′) resulted in –3 deletion mutations, presumably due to the weakly paired A:T region around the lesion. However, the structural/conformational bases of these deletion mutations remain elusive.

In the present study we created fully paired, -3, -2 and -1 bulge duplexes using a fluorine containing AAF (FAAF) in a 16-mer template (5′-CTCTCG<u>AT</u>G*CCATCAC-3′). This sequence is identical to the core sequence used by the abovementioned paper by Schorr et al. that caused -3 frameshift mutations (Figure 4a-d). In addition, we created an

AAF modified -1 deletion duplex (Figure 4e) using a different 16-mer template (5′-CTCTCGGCG*CCATCAC-3′) by replacing ‘AT’ in the first sequence by ‘GC’ to see the difference in the conformational profiles between ‘AT’ -1 deletion (TG*C) and ‘GC’ -1 (CG*C) deletion duplexes.

We hypothesize that the AAF-lesion exists in a mixture of two major conformations: the stable intercalated and the unstable external conformers. The combined thermodynamic stabilities play a critical role in determining the different outcomes of deletion mutations. We have utilized dynamic ^{19}F NMR and CD spectroscopy to investigate the conformational profiles of several AAF-containing model deletion duplexes. Furthermore, we employed UV-melting and differential scanning calorimetry (DSC) to study their thermodynamic properties. The results present valuable structural and thermodynamic evidences for the manifestation of various frameshift mutations.

CHAPTER II

MATERIALS AND METHODS

Caution: 2-Acetylaminofluorene derivatives are mutagens and suspected human carcinogens and therefore must be handled with caution.

Crude oligodeoxynucleotides (ODNs, 10 μmol scale) in desalted form were purchased from Eurofins MWG Operon (Huntsville, AL, USA). All HPLC solvents were purchased from Fisher Inc. (Pittsburgh, PA, USA).

Preparation and characterization of FAAF modified ODNs

FAAF-modified 16-mer ODNs were prepared using the general procedures described previously (*22, 30*). For example, 0.5 ~ 1 mg of *N-acetoxy-N-2-(acetyl amino)-7-fluorofluorene* which was prepared from starting material 7-fluoro-2-nitrofluorene, was dissolved in absolute ethanol was added drop wise to a pH 6.0 sodium citrate buffer (10mM) containing unmodified oligomer (5′-CTCTCG$_1$ATG$_2$CCATCAC-3′) and placed in a water-bath shaker for 5 min at 37°C. Figure 5a shows a typical reverse-phase HPLC chromatogram derived from an aliquot of the reaction mixture. Unmodified oligomer appeared at 11.7 min and modified oligomers, two mono-adducts and one di-adduct, between 15 and 25 min. The two mono FAAF-modified oligos were separated and purified up to >97% purity by repeated injections on HPLC. The HPLC system consisted of a Hitachi EZChrom Elite HPLC unit with an L2450 diode array detector and a Phenomenex Luna C18 column (150×10 mm, 5.0 μm). We employed a gradient system involving 3–15% Acetonitrile for 15 min followed by 15–30% acetonitrile for 25 min,

respectively, in pH 7.0 ammonium acetate buffer (100 mM) with a flow rate of 2.0 ml/min. The FAAF-modified G_2 (5′-CTCTCG$_1$ATG$_2$(FAAF)CCATCAC-3′) was annealed with an appropriate complementary sequence (5'-GTGATGGCATCGAGAG-3') to form a fully paired duplex. Deletion duplexes (-3, -2, and -1) (Figure 4 a-d) and an identical set of unmodified control duplexes were similarly prepared.

Characterization of FAAF modified oligomers

FAAF-modified 16-mer oligos were characterized by initial enzyme digestions followed either by matrix assisted laser desorption ionization-time of flight (MALDI-TOF) or eletrospray ionization (ESI) LC/MS detection.

Enzymatic digestion/MALDI-TOF

A matrix solution was prepared by dissolving a 1:1 ratio of 3-hydroxypicolinic acid (3-HPA) and di-ammonium hydrogen citrate (DHAC). 1 µL of each analyte and the matrix solution were mixed to produce a spotting solution. 1 µL of the spotting solution was spotted on the MALDI plate and air dried.

A 1 µL sample containing 100 pmol of the FAAF modified 16-mer oligo was used in both snake venom phosphodiesterase (SVP) and bovine spleen phosphodiesterase (BSP) digestion experiments. SVP and BSP remove one nucleotide at a time from the 3'- or 5'-end, respectively. For the SVP digest, 0.5-2 µL of SVP solution (10×10^{-2} units/ µL) was added to 1 µL of the oligonucleotide solution, 6 µL of 100 mM ammonium citrate, and 6 µL of deionized water. In the BSP digestion, 1-2 µL BSP (1×10^{-2} units/ µL) solution was added to 1 µL of the oligonucleotide solution and 7 µL of deionized water.

The digest solution was heated to 37 ℃ for the SVP digestion, but kept at room temperature for the BSP digestion. A 1 μL sample of the digest solution was removed at regular time intervals until the digestion rate was significantly reduced, and the reaction was quenched by mixing the aliquot with 1 μL of matrix (3-HPA and DHAC in 1:1 ratio). The sample was spotted on the MALDI plate and dried for immediate analysis. All MALDI-MS spectra were obtained using Shimadzu mass spectrometer in the Reflectron-mode. Oligonucleotide molecular weight and detection limit determinations required 10 shots from the nitrogen laser (337 nm), whereas 150 laser shots were summed when the digest was analyzed.

***Enzymatic digestion*/ESI-LC/MS**

We used electrospray ionization and quadrupole time-of-flight (TOF) mass spectrometry to verify the molecular weights and the position of FAAF attachment on the 16-mer oligomer. The ESI technique is used to produce intact highly charged molecular ions of oligo, as it can overcome the propensity of these molecules to fragment when ionized (*31*). For oligos with high molecular weight, this ionization results in a characteristic bell-shaped distribution of multiply charged ions. Along with such a distribution, it is also accompanied by an adjacent major peak in the spectrum differing by one charge.

The FAAF-modified 16-mer oligomers were sequenced using 3′→5′ or 5′→3′ exonucleases as described previously for the analysis of modified 12-mers (*31*). Briefly, 1 μg of a 16-mer template was combined with 0.01 units of an exonuclease in a 1 mM solution of $MgCl_2$ and incubated for several hours. The digest was separated using a Phenomenex Aqua C18, 1.0×50 mm column (5 μm; 120A˚). Solvent A was 5 mM in both ammonium acetate and dimethylbutyl amine. Acetic acid was added to solvent A to

adjust the pH to 7.0. Solvent B was 0.1% formic acid in acetonitrile. The flow rate was 100µl/min and the total run time was 20 min. All LC/MS spectra were acquired using a Waters SYNAPT quadrupole time-of-flight mass spectrometer (Milford, MA, USA) operated in the negative ion and V-modes.

UV-melting

UV melting data were obtained using a Cary100 Bio UV/VIS spectrophotometer equipped with a 6×6 multi-cell block and 1.0 cm path length. Sample cell temperatures were controlled by an in-built Peltier temperature controller. Samples with a total concentration in the range of 0.5–10 µM were prepared in solutions containing 0.2 M NaCl, 10 mM sodium phosphate and 0.2 mM EDTA at pH 7.0. Thermomelting curves were constructed by varying temperatures of the sample cell (1 °C/min) and monitoring absorbances at 260 nm. A typical melting experiment consisted of forward/reverse scans and was repeated five times. Thermodynamic parameters were calculated using the program MELTWIN version 3.5, as described previously (*32*).

Circular Dichroism (CD)

CD measurements were conducted on a Jasco J-810 Spectropolarimeter equipped with a Peltier temperature controller. Typically, 6.5 µM of each strand were annealed with an equimolar amount of a complementary sequence. The samples were dissolved in 300 µl of a pH 7.0 buffer (0.2 M NaCl, 10 mM sodium phosphate, 0.2 mM EDTA) and placed in a 1.0 mm path length cell. The samples were heated at 85 °C for 5 min and then cooled to 15 °C, over a 10 min period to ensure complete duplex formation. The spectropolarimeter

was scanned from 200 to 400 nm at a rate of 50 nm/min. Spectra were acquired every 0.2 nm with a 2 s response time were the averages of 10 accumulations and were smoothed using 17-point adaptive smoothing algorithms provided by Jasco.

Dynamic ^{19}F Nuclear Magnetic Resonance (^{19}F-NMR) Spectroscopy

Approximately 20 ods of the G_2-FAAF-modified 16-mer ODN (5′-CTCTCGATG[FAAF] CCATCAC-3′) were annealed with an equimolar amount of the respective complementary sequence to produce fully paired, -3 deletion, -2 deletion, -1 deletion duplexes (Figure 3a-d). Similarly, a FAAF-modified 16-mer *Nar*I Sequence (5′-CTCTCGGCG[FAAF]CCATCAC-3′) was annealed with an equimolar amount of the respective complementary sequence to produce 'GC'-1 deletion duplexes. The samples were then dissolved in 300 µl of a pH 7.0 NMR buffer containing 10% D_2O/90% H_2O, 100 mM NaCl, 10 mM sodium phosphate and 100 mM EDTA, and filtered into a Shigemi tube through a 0.2 mm membrane filter. All ^{1}H- and ^{19}F-NMR results were recorded using a HFC probe on a Varian NMR spectrometer operating at 500.0 and 476.5 MHz, respectively, using acquisition parameters described previously (*33*-*35*). ^{19}F-NMR spectra were acquired in the ^{1}H-decoupled mode and referenced relative to that of $CFCl_3$ by assigning external C_6F_6 in C_6D_6 at -164.9 ppm. One and two-dimensional ^{19}F-NMR spectra were measured between 5 and 78°C with increment of 5–10°C. Temperatures were maintained by a Bruker-VT unit with the aid of controlled boiling liquid N_2 in the probe. Computer line shape simulations were performed as described previously (*36*) using WINDNMR-Pro (version 7.1.6; J. Chem. Educ. Software Series; Reich, H.J., University of Wisconsin, Madison, WI, USA).

Differential Scanning Calorimetry (DSC)

Microcalorimetric measurements of all five FAAF-modified 16-mer duplexes were performed using a Nano-DSC from TA Instruments (Lindon, UT, USA). Prior to temperature scanning, samples were degassed for at least 10 min under vacuum in a closed vessel. Solutions were loaded, respectively, into the sample and reference cells using a pipette by attaching a small piece of silicone tube at the end of the tip and were purged several times to get rid of air bubbles. After both cells were filled, they were capped and a slight external pressure (~3 atm) was applied to prevent evaporation of the sample solution. Raw data were collected as microwatts versus temperature. Template-primer solutions were prepared by dissolving desalted samples in a pH 7.0 buffer solution consisting of 20 mM sodium phosphate and 0.1 M NaCl. In a typical scan, a 0.1 mM template-primer solution was scanned against buffer from 15 °C to 90 °C at a rate of 0.75 °C/min. At least five repetitions were obtained. A buffer vs. buffer scan was used as a control and subtracted from the sample scan and normalized for heating rate. This results in base-corrected ΔC_p^{ex} versus temperature curves. Each transition showed negligible changes in the heat capacities between the initial and final states, thus was assumed to be zero. The area of the resulting curve was proportional to the transition heat, which, when normalized for the number of moles of the sample, is equal to the transition enthalpy, ΔH. ΔH is an integration of ΔC_p^{ex} over temperature T. All sample solutions were 0.1 mM concentration. Tm is defined as the mid temperature point of the double-strands to single strands. ΔG and ΔS values have been determined according to the procedures described by Chakrabarti et al. (*37*).

CHAPTER III

RESULTS

Model Systems

As model systems, we used 16-mer DNA template (5′-CTCTCG$_1$ATG$_2$*CCATCAC-3′), in which G* was modified by FAAF (Figure 3b). This template was annealed with four different length primers to prepare four model duplexes [designated as fully paired (16/16-mer), -3 deletion (16/13-mer), -2 deletion (16/14-mer) and -1 deletion (16/15-mer) duplexes respectively] (Figure 4 a-d).

Figure 5a shows the reserve-phase HPLC profile of a work-up mixture after 20 min of reaction. Unreacted control oligo appeared as peak 1 at 11.7 min, which is followed by three FAAF-modified ODNs (peaks 2, 3 and 4) in the 15 - 25 min time period. Online UV (Figure 5b) of the modified ODNs displayed a small shoulder in the 290-320 nm range, which is in contrasted with the unmodified control peak 1 which shows no such shoulder in that area. Peaks 2 and 3 were assigned to mono-FAAF adducts and peak 4 as the di-adduct based on their UV intensity ratios in the 290-320 nm region and exonuclease digestion/MALDI-TOF and ESI-TOF-MS-MS analyses (see below).

In addition, we used a different FAAF-modified 16-mer template (Figure 3c) G$_3$ (5′-CTCTCG$_1$G$_2$CG$_3$*CCATCAC-3′) to prepare a ‘GC’-1 deletion duplex (Figure 4e). This modified sequence has been characterized previously (*38*).

Matrix-Assisted Laser Desorption Ionization-Time of Flight (MALDI-TOF)

The molecular weights of the two FAAF mono-adducts (Peak 2 and Peak 3) were measured by MALDI-TOF prior to sequence verification by exonuclease digestions. Exonucleases cleave terminal deoxynucleotides from the oligo chain until the FAAF-modified nucleotide is exposed at the end of the chain. At that point the digestion reaction slows down significantly. The position of modification is identified (in this case) when the fragment(s) formed by the loss of the unmodified guanine nucleotides is observed in the MALDI-TOF spectra. Peaks 2 and 3 were characterized as G_1 and G_2, respectively.

a) 5′→ 3′ exonuclease digestion of Peak 2:

Figure 6 shows the 5'→3' exonuclease digestion fragments for peak 2 at different time intervals. The ions observed at m/z 5016 in 6(a) represent the FAAF modified 16mer oligo (5'-CTCTCG$_1$ATG$_2$CCATCAC-3') before adding BSP enzyme. As shown in Figure 6 (b, c, d) increase in incubation time leads to the digestion of the subsequent unmodified bases. However, 5'-digestions was significantly slowed down at m/z 3,540. The m/z 3540 ion at 60 min of 5'-digestion represents an ion formed from the FAAF modified 5'-G$_1$(FAAF)ATG$_2$CCATCAC-3' fragment (see inset for theoretical MW values), suggesting peak 2 is a G_1 position of the FAAF modified 16-mer template.

b) 3′→ 5′ exonuclease digestion of Peak 2:

Figure 7 represents the 3'→5' exonuclease digestion fragments for peak 2 at different time intervals. The ions observed at m/z 5,016 in Figure 7(a) represents an ion

of the FAAF modified 16-mer ODN (5'-CTCTCG$_1$ATG$_2$CCATCAC-3') before adding SVP enzyme. As shown in Figure 7 (b, c, d), increase in incubation time leads to the digestion of the subsequent unmodified bases. Compared to 5', the 3' digestion takes place in few minutes. The 3'-digestion was significantly slowed down at m/z 1,982 at 2 and 5 min indicating the presence of the AAF lesion. The m/z 1982 ion at 5 min of 3'-digestion represents an ion formed from the FAAF modified 5'-CTCTCG$_1$(FAAF)-3' fragment (see inset for theoretical MW values) suggesting peak 2 is a G_1 position of the 16-mer template.

c) 5′→ 3′ exonuclease digestion of Peak 3:

Figure 8 represents the 5'→3' exonuclease digestion fragments for peak 3 at different time intervals. The ions observed at m/z 5,016 in 8(a) represent ion from the FAAF modified 16mer oligo (5'-CTCTCG$_1$ATG$_2$CCATCAC-3') before adding BSP enzyme. As shown in Figure 8 (b, c, d) increase in incubation time leads to the digestion of the subsequent unmodified bases. However, 5'-digestions were significantly slowed down at m/z 2,593. The ion m/z 2,593 at 60 min of 5'-digestion represents the ion formed from the FAAF modified 5'-(FAAF)G$_2$CCATCAC-3' fragment (see inset for theoretical MW values), suggesting that peak 3 is a G_2 position of the 16-mer template.

d) 3′→ 5′ exonuclease digestion of Peak 3:

Figure 9 represents the 3'→5' exonuclease digestion fragments for peak 3 at different time intervals. The ions observed at m/z 5,016 in 9(a) represent ions from the 16-mer FAAF modified 16mer oligo (5'-CTCTCG$_1$ATG$_2$CCATCAC-3') before adding SVP enzyme. As shown in Figure 9 (b, c, d) increase in incubation time leads to the digestion

of the subsequent unmodified bases. The 3'-digestion was significantly slowed down at m/z 2,928 at 30 sec, 2 and 5 min. The ion m/z 2,928 of 3'-digestion represents ion formed from the FAAF modified 5'-CTCTCG$_1$ATG$_2$ (FAAF)-3' fragment (see inset for theoretical MW values) suggesting the peak 3 is a G$_2$ position of the 16-mer template.

Electro Spray Ionization Quadruple Time of Flight (ESI-QTOF)-mass spectrometry

The molecular weights of FAAF-modified oilgos were measured by ESI-QTOF-MS prior to sequence verification by exonuclease digestion. Exonucleases cleave terminal deoxynucleotides from the oligo chain until the FAAF-modified nucleotide is exposed at the end of the chain. At that point the digestion reaction slows down significantly. This is shown in Figure 10(a) for the 5'→3' digest of the 16-mer template 5' -CTCTCG$_1$ATG$_2$CCATCAC-3'. The ions observed at m/z 1178 is the $(M-3H)^{3-}$ ion from the fragment 5'-G$_1$(FAAF)ATG$_2$CCATCAC-3'. The observation of these ions confirms that peak 2 is modified on the G$_1$ closest to the 5' end. Figure 10(b) shows the LC/MS analysis of the 3'→5' digest of the modified oligo. The ions at m/z 989 correspond to the $(M-2H)^{2-}$ ion formed from the fragment 5'-CTCTCG$_1$(FAAF)-3', confirming that this oligo is modified on the guanine closest to the 5' terminus. The observation of oligo fragments with two G's in both 3' and 5' digests confirms that the peak 2 is G$_1$.

Figure 11(a) corresponds for the 5'→3' digest of the peak 3. The ions observed at m/z 863 and m/z 1295 are the $(M-3H)^{3-}$ and $(M-2H)^{2-}$ ions from the fragment 5'-G$_2$(FAAF)CCATCAC-3'. The observation of these ions confirms that this peak 3 is modified on the G$_2$. Figure11 (b) corresponds to the LC/MS analysis of the 3'→5' digest of the modified oligo. The ions at m/z 975 and m/z 1463 correspond to the $(M-3H)^{3-}$ and

$(M-2H)^{2-}$ ions formed from the fragment 5'-CTCTCG$_1$TAG$_2$(FAAF)-3', confirming that this oligo is modified on the guanine closest to the 3' terminus. From ESI-QTOF-MS experiments, peaks 2 and 3 were characterized as G_1 and G_2 respectively.

UV-melting

Figure 12(a-e) shows the UV melting profiles of the five FAAF duplexes relative to their respective unmodified control duplexes, all at 10 μM. All duplexes showed typical monophasic, sigmoidal, helix-coil transitions with a strong linear correlation (R^2>0.9) between T_m^{-1} and lnC_t. Thermal and thermodynamic parameters calculated from UV-melting are summarized in Table 1. In case of the full and -3 deletion duplexes, modified duplexes were destabilized thermally and thermodynamically, respectively, relative to their respective unmodified duplexes: full duplex (-7.7 ^oC, 4.5 kcal/mol, respectively) > -3 deletion (-5.7^oC, 2.0 kcal/mol). By contrast, -2 deletion and 'AT'-1 deletion duplexes displayed thermal and thermodynamic stabilization: 'AT' -1 deletion (13 ^oC, -8.5 kcal/mol, respectively) > -2 deletion (9.5 ^oC, -7.2 kcal/mol, respectively), whereas destabilization was in the order of Full duplex (-7.7 ^oC, 4.5 kcal/mol, respectively) > -3 deletion (-5.7 ^oC, 2.0 kcal/mol, respectively). Both 'AT' and 'GC' -1 deletion duplexes displayed similar thermal and thermodynamic stabilization. The small differences between the two could be due to difference in conformational characteristics.

Differential Scanning Calorimetry (DSC)

Figure 13(a-e) shows DSC plots of excess heat capacity C_p^{ex} vs. temperature for all five modified duplexes relative to their unmodified controls. Table 2 summarizes the thermal and thermodynamic parameters derived from these DSC curves. The median

peak of each bell curve indicates a melting temperature (T_m), at which half a duplex denatures, whereas the areas under the curve represents enthalpy (ΔH) of duplex formation. Consistent with the UV melting data, the 'AT'-1 deletion duplex was most stabilized, ($\Delta\Delta G_{37°C}$ = -6.3 kcal/mol, ΔT_m = 15.2 °C), followed by -2 deletion duplex ($\Delta\Delta G_{37°C}$ = -3.5 kcal/mol, ΔT_m = 10.8 °C). As expected, the fully paired FAAF-modified duplex was most destabilized ($\Delta\Delta G_{37°C}$ = 3.5 kcal/mol, ΔT_m = -8.0 °C) followed by -3 deletion duplex ($\Delta\Delta G_{37°C}$ = 0.8 kcal/mol, ΔT_m = -3.1 °C).

The differences in the thermal and thermodynamic parameters among the modified duplexes must have arisen from their differences in the conformational characteristics. It is well known in the fully paired arylamine modified duplexes that the syn glycosidic stacked (S) and the minor groove binding wedge (W) conformers induce thermodynamic destabilization. By contrast, inserted/carcinogen stacked conformation in the bulge duplexes has shown to increase thermal and thermodynamic stability. For example, a dramatic thermal stabilization has been observed for several bulge duplexes modified by the bulky arylamine and benzo[a]pyrene carcinogens. For example, the highly stacked conformeric 'AT' (72%) and 'GC' -1 (73%) deletion duplexes (*39*) would decrease entropy ($\Delta\Delta S$ = -50.8eu and -20.0 eu respectively), which is compensated by large enthalpies ($\Delta\Delta H$ = -21.9 Kcal/mol and $\Delta\Delta H$ = -9.6 Kcal/mol respectively). The net result is a gain in overall free energy ($\Delta\Delta G_{37°C}$ = -6.3 kcal/mol and $\Delta\Delta G_{37°C}$ = -3.5 kcal/mol respectively). In contrast, -3 deletion duplex possessing a greater external conformation (52%) displays an entropy gain ($\Delta\Delta S$ = 8.4 eu), but is compensated ($\Delta\Delta H$ = 3.5 Kcal/mol) to produce an overall loss of free energy ($\Delta\Delta G_{37°C}$ =0.8 kcal/mol). As for the fully-paired duplex, 60% of S-conformations causes disturbance of Watson-crick base

pairing, resulting in enthalpy reduction ($\Delta\Delta H$ = 13.9 Kcal/mol). Again, enthalpy-entropy compensation resulted in loss of free energy ($\Delta\Delta G_{37°C}$ = 3.5 kcal/mol) (*39*). The DSC thermograph in Figure 14 shows the differences in thermal and thermodynamic parameters of these deletion duplexes.

As expected, both the "AT' and 'GC' -1 duplexes exhibited high stacked conformer population (72-73%) (see below ^{19}F NMR), thus displaying greater thermal and thermodynamic stability. Compared to 'AT', the 'GC' -1 deletion duplex displayed slightly higher ΔT_m possibly due to the greater hydrogen bonding strength of G:C vs. A:T. (Figure 17: c, d).

Induced Circular Dichroism (ICD)

Figure 15(a-e) shows the overlay CD spectra at 30 ℃ of all the duplexes in both unmodified and FAAF-modified. All duplexes exhibited a CD pattern characteristic for B-form DNA duplexes with positive and negative S-shaped ellipticity curve at around 275 and 250 nm, respectively. Modified duplexes displayed low intensity shoulders in the narrow 290-320 nm range, which is characteristic of FAAF modification (*30, 38, 40*).

A slight increase in the positive intensity (hyperchromity) around 275 nm was observed for the FAAF modified (red) -2 deletion, 'AT' -1 deletion, 'GC'-1 deletion duplexes relative to their unmodified duplexes (blue) respectively. This may be due to adduct-induced stability caused by increase in stacking interactions in the bulged pocket. However, the opposite (hypochromity) is true for the full and -3 deletion duplexes with the effect much greater for the latter. The difference in stability is likely due to the differences in conformational populations (inserted/stacked vs. external binding). These

adduct- induced stabilization/destabilization was supported by the thermodynamic data described above.

CD Blue shifts:

In addition to the conformation specific ICDs above, the modified duplexes also displayed significant blue shifts relative to their respective unmodified duplexes (Figure 15, Table 3). With the exception of -3 deletion duplex, all other modified duplexes exhibited significant blue shifts (up to 5 nm). The order of blue shift was in order of full duplex ($\Delta_{G^*\text{-}G}$ =5nm) > 'AT'-1 deletion ~ 'GC' -1 deletion ($\Delta_{G^*\text{-}G}$=4nm) > -2 deletion ($\Delta_{G^*\text{-}G}$ =3nm). We previously reported that a FAAF-modified duplex in the CG*C context exists mostly (61%) in the stacked conformation. As a consequence, the greater CD blue shift in the full duplex could be due to the disturbance of Watson and Crick base pairing at the lesion site. These blue shifts could also indicate a lesion- induced distortion of DNA backbone contributing to bending (*41*). The next higher blue shifts seen in both 'AT' and 'GC' -1 deletion duplexes followed by -2 deletion duplex also could be based on the percentage of stacked conformations which are 72 and 73% in the 'AT' and 'GC' -1 duplexes respectively and 55% in the -2 deletion duplex.

CD Red shift:

As shown in Figure 15b, the FAAF modified -3 deletion duplex displayed a shift to longer wavelengths at 270 nm ($\Delta_{G\text{-}G^*=}$3nm). This red shift could have arisen due to a high percentage of external conformations (52%) compared to other deletion duplexes.

Figure 16 shows an overlay of the CD spectra for the four FAAF modified (1 full- and -3 deletion) duplexes relative to fully unmodified duplex as a control. The idea was

that unmodified deletion duplexes alone could not be used as a proper control. We observed similar order of blue shifts in all duplexes (Table 4). Here, -3 deletion duplex actually displayed a blue shift, not the red shift as in Figure 14b. The blue shift was in the order of full duplex ($\Delta_{G^*\text{-}G}$ =5nm) > 'AT' -1 deletion ($\Delta_{G^*\text{-}G}$ =4nm) > -2 deletion ($\Delta_{G^*\text{-}G}$ =3nm) ~ -3 deletion ($\Delta_{G^*\text{-}G}$ =3nm). A greater negative dip at 290-320nm range was seen for the full duplex followed by -1, -2 ~ -3 deletion duplexes.

Dynamic ^{19}F NMR

Figure 17 shows the dynamic ^{19}F NMR spectra (5-78°C) of FAAF-modified duplexes in four different sequence settings (fully paired, -3, -2, 'AT'-1 deletion, 'GC' -1 deletion) from -111 to -120 ppm. The signals in these duplexes coalescence into a single signal at different temperatures depending upon their duplex stability (70, 60, 65, 75, 78 ^{o}C for fully paired, -3, -2, 'AT' -1, 'GC' -1 deletion duplexes respectively). All signals coalesced at around -114.50 ppm, which signifies a complete duplex melting.

Conformational Heterogeneity: ^{19}F NMR Signal Assignment

We previously reported ^{19}F NMR studies of fully paired FAAF-modified duplexes with various flanking sequence contexts (TG*A, CG*C, CG*G, GG*C) and in different length (11- and 16-mer). The results showed that FAAF-duplexes exist in a mixture of B, S and W conformations going from downfield to up field, i.e., -115.0 to -115.5 ppm, -115.5 to -117.0 ppm and -116.5 to -118.0 ppm, respectively (*30*). Using this general strategy, we assigned the two distinct signals at -115.6 and -117.9 ppm in the FAAF-modified fully paired 16-mer duplex at 5°C as 'S' and 'W' conformations (*30*).

The major ^{19}F signals in both 'AT' and 'GC' -1 deletion duplexes seem to fit into that pattern. The 'GC' -1 deletion duplex displayed two major signals at 10 °C. The signal at -115.7 ppm could be assigned as external binding conformer (B-type) because of its downfield shift and close proximity to the single stranded signal at -114.5 ppm at 78 °C. The shielding signal at -116.3 ppm is resistant to melting, thus showing a signal at even at 70 °C. This is typical for an inserted/stacked (S type) conformation. The 'GC' -1 duplex undergoes a major melting transition around 70 °C. The high coalescence melting behavior of the 'GC' -1 duplex is consistent with the greater thermal and thermodynamic stability measured by UV melting (Table 1) and DSC (Table 2) data.

The 'AT' -1 deletion duplex exhibited a similar ^{19}F NMR pattern as the 'GC' one and was assigned accordingly, i.e., external B (-115.5 ppm) and inserted S (-116.5 ppm). The signal at -116.1 ppm (marked in asterisk) is located in between S and B and coalesced with the stacked conformation above 40°C. This signal could be an intermediate conformer between B and S, but we were unable to pinpoint assignment. Again, the greater stability of the 'GC' over 'AT' -1 duplex must be due to the better hydrogen-bonding capability of the 5'-G:C over A:T.

The -3 and -2 deletion duplexes also displayed two major ^{19}F signals in the -114 ~ -115 and -114.5 ~ -115.5 ppm range, respectively. However, these signals are collectively shifted to the downfield by about 1 ppm relative to those of -1 duplexes, suggesting an altered electronic environment. The major signals could be assigned as an external B (downfield) and stacked S (upfield) conformations according to their chemical shifts. However, we were unable to identify the additional signals marked as asterisk (Figure 17).

Figure 18 shows ^{19}F NMR spectra at 30°C. The percent population ratios were calculated on the basis of computer line simulations. The external B and stacked S conformer population ratios for the FAAF modified -3, -2, -1 and 'GC' -1 deletion duplexes were found to be 52:37, 37:55, 10:72 and 27:73 respectively. In the full duplex, the ratio of stacked (S) and wedge (W) conformations was 60:40. The population of S conformers was in the order of 'GC'-1 deletion ~'AT' -1 deletion > full duplex > -2 deletion > -3 deletion and that of external-conformer is -3 deletion > -2 deletion > 'GC' -1 deletion > 'AT'-1 deletion.

Lesion-induced thermodynamic stabilization in the bulge structures are also evident from the dynamic imino proton spectra shown in Figure 19. At 5 °C, a mixture of broad imino signals were observed not only from those involved in Watson-Crick hydrogen bonds (12~14 ppm), but also those at and near the lesion site (~11 ppm). We also performed the temperature dependence of the imino proton spectra at 5, 20, 30, 40 ℃ and compared with the unmodified control duplexes (Figure 20, 21). Unlike the full duplex, the high field imino proton signals of the -3 deletion duplex disappeared rapidly as the temperature increase, indicating adduct-induced conformational flexibility at and near the lesion site. The deletion duplexes, particularly the -1, showed strong presence of those high field imino protons even at higher temperatures, indicating tightly packed lesion structures, inducing thermodynamic stabilization.

Milhe et al. reported a 70% major external B conformation for the 11/10-mer in the CG*C sequence context, in which the AAF[G] is opposite a -1 deletion site (*23*). This is in contrast to the present results for the longer 16/15-mer duplex with the same CG*C context that showed 73% S conformation. However, Mao et al have reported an

exclusive base displaced stacked S conformation for the N-deacetylated AF opposite a -1 deletion site in an 11/10-mer duplex (*25*).

CHAPTER IV

DISCUSSION

In this study, we investigated the role of conformational heterogeneity on thermal and thermodynamic stability of bulge duplexes modified with the prototype bulky arylamine FAAF. It is believed that the bulge structures are implicated in frameshift mutagenesis in the form of the so-called "slipped mutagenic intermediate (SMI)." A working hypothesis is that the conformational and thermodynamic stability of a SMI is a key factor for determining the extent of the frameshift mutations. We also hypothesized that deletion duplexes can exist in three major conformational motifs: external binding anti-glycosidic B, syn-glycosidic inserted stacked S, and others between B and S. To that end, we chose the three duplexes shown in Figure 2 as model systems for -1, -2, and -3 deletion mutations. As for -1 deletion, we studied two 5'-sequence context: AT vs. GC base pair. We conducted a variety of spectroscopic (CD, UV, NMR) and calorimetric (DSC) studies to obtain the conformational and structural information.

The ^{19}F-NMR results show that FAAF in the model duplexes exists in varying ratios of mixture of B and S conformers. A greater population of the bulge stacked conformation was observed in 'GC' (73%) and 'AT' (72%) -1 deletion duplexes than the -2 (55% S) and -3 (37% S) counterparts. As such, the highly stacked -1 bulged duplexes were greatly stabilized relative to -2 and -3 bulged duplexes, due to favorable stacking interactions between the intercalated fluorene and the bulge. These results were supported by increased positive CD at 275 nm, which indicated increased π-π stacking

interactions between fluorene and DNA base pairs. We also observed a lesion induced blue CD shift, which is characteristic for lesion-induced DNA bending.

^{19}F NMR shows that the -3 deletion duplex exists in a mix of 55% B and 37% S conformers. Accordingly, the CD of the -3 duplex exhibited a red shift (Figure 15b) and hypochromic effect at 270 nm. This suggests a decrease in π-π stacking interaction of the intercalated aminofluorene in the flexible bulge, consistent with high percentage of external B conformer. Unlike bulge duplexes, where a stacked conformation stabilizes the bulge, the highly populated stacked conformations (60%) in the full duplex actually disrupts the Watson-Crick base pairing at the lesion site causing a greater blue shifts and a hypochromic effect in CD (*40*). The -2 and -3 deletion duplexes exhibited comparatively smaller blue shifts, suggesting lesser disturbance of the double helical structure. However, the full duplex displayed a greater blue shift compared to the bulged structures although the population of stacked conformations (60%) in the full duplex were low compared to -1 bulged structure (72%). As a result, stacked conformation displays greater DNA bending in the full duplex, but promotes stability in the bulged structures.

As expected, FAAF in fully paired duplex resulted in thermal and thermodynamic destabilization relative to the unmodified control duplex. It has been documented that N-acetylated FAAF adducts in fully paired duplexes produce a mixture of complex S/B/W- conformers (*30*). The N-acetyl group is responsible for generating up to 40% W- conformers in the present 16-mer non *Nar*I sequence (Figure 17a). We were unable to find the B conformation in the fully-paired duplex. The destabilizing effect of FAAF was related to the difference in the conformational populations. Thus, the

presence of 60% S-conformations in full duplex promoted lesion stacking and disrupted the Watson-Crick base pairs, resulted in thermal (ΔT_m = -8.0 °C) and enthalpy destabilization ($\Delta\Delta H$ = 13.9 Kcal/mol). Our previous studies of conformational and thermodynamic studies on *Nar*I 16-mer full duplex also displayed 61% S-conformations, resulting in thermal (ΔT_m = -8.3 °C) and enthalpy destabilization ($\Delta\Delta H$ = 24.7 Kcal/mol) (*40*). In contrast to the full duplex, the stacked conformer in bulged duplexes resulted in thermal and thermodynamic stabilization. Theoretical studies suggested that the syn-glycoside conformeric SMI is more stable than the external conformation and can be stabilized by many favorable interactions between a carcinogen and flanking base pairs inside the bulging pocket (*19*). In both 'GC'-1 deletion duplex and 'AT' -1 deletion duplexes, the highly stacked conformeric (73 and 72% respectively) exerted enthalpy stabilization ($\Delta\Delta H$ = -15.2 Kcal/mol and $\Delta\Delta H$ = -21.9 Kcal/mol respectively). The -2 deletion duplex displayed intermediate thermal (ΔT_m = -9.6°C) and enthalpy stabilization ($\Delta\Delta H$ = -9.6 Kcal/mol) which could be due to the presence of the intermediate population of stacked conformers (55%). Our previous work on the *Nar*I -2 deletion duplex displayed thermal (ΔT_m = 11.7°C) and enthalpy stabilization ($\Delta\Delta H$ = -5.3 Kcal/mol). As expected, the high external conformations (52%) and low stacked conformer populations (37%) in the -3 deletion duplex exerted destabilization in enthalpy ($\Delta\Delta H$ = 3.5 Kcal/mol) (*34*).

Biological implications:

Translesion DNA synthesis and subsequent elongation are most likely achieved by employing specialized lesion-bypass polymerases (*15*). Using gel based primer kinetics, Schorr et al have shown the mechanism of dG-C8-AAF induced frameshifts by

the human DNA polymerase η. The lesion could base pair correctly with dC causing -1, -2 and -3 frameshifts depending upon the base pairs around the lesion (Figure 22). The band representing the -1 frameshift appears to be more pronounced (Figure 22a), followed by the -2 frameshift which also showed several shorter sequences as well as the fully replicated 20-mer sequence. This is followed by -2 and -3 frameshift products (Figures 22 b and c). This is in accordance with our thermodynamic data where the -1 deletion duplex displayed high stability followed by -2 and -3 deletion duplexes. These results support the importance of lesion stacking which is directly correlated to mutational efficiencies.

Our working hypothesis is that the conformational and thermodynamic stability of adduct-induced bulge is a key determining factor for the propensity to form frameshift mutations. Fuchs et al studied the mechanism of AAF mutagenesis by DNA sequencing the spectrum of mutations in the *E.coli* lacI gene and found a greater frequency of -2 followed by -1 frameshifts, and few -3 deletions were observed (*42*). The ^{19}F NMR data showed that the AAF- modified opposite -1, -2 and -3 deletion duplexes have revealed 72%, 55% and 37% of stacked S conformation. We found that the -1 and -2 deletion duplexes are stacked better, having tight compactness of the lesion in the bulge, consequently displaying a greater stability. In the -3 deletion duplex, however, the lesion is not stacked well, resulting in more conformation flexibility. These results indicate that optimum space required to incorporate the AAF lesion is -1 followed by -2 bulge, in agreement with the extension assay data (Figure 22).

Table 1: Thermal and thermodynamic parameters from UV-melting curves

	-ΔH Kcal/mol		-ΔS eu		-ΔG37℃ Kcal/mol		T_m [b] ℃		ΔΔH[C] Kcal/mol	ΔΔS[d] eu	ΔΔG[e] 37℃ Kcal/mol	ΔTm[f] ℃
	Um	Mod	Um	Mod	Um	Mod	Um	Mod				
Full duplex	122.3	101.0	333.2	279.0	19.0	14.5	62.0	55.3	21.3	54.2	4.5	-7.7
-3 deletion	99.0	88.7	276.6	248.9	13.3	11.5	52.2	46.5	10.3	27.7	2.0	-5.7
-2 deletion	93.0	114.8	262.7	319.7	11.5	15.7	47.0	56.5	-21.8	-57.0	-7.2	9.5
'AT' -1 deletion	100.2	122.5	280.0	341.4	13.3	21.8	52.0	65.0	-22.3	-61.4	-8.5	13.0
'GC' -1 deletion	103.1	123.7	282.9	340.3	15.4	17.5	53.7	67.0	-20.6	-57.4	-7.1	13.3

Blue: Unmodified, Red: Modified

a) The average standard deviation for –ΔG, -ΔH and T_m [b] are ± 0.4, ± 3.0 and ± 0.4 respectively.
b) T_m value is the temperature at half the peak area.
c) $\Delta\Delta H^c = \Delta H$(modified duplex) - ΔH(Control)
d) $\Delta\Delta S = \Delta S$(modified duplex) - ΔS(Control)
e) $\Delta\Delta G = \Delta G$(modified duplex) - ΔG(Control)
f) $\Delta T_m = T_m$ (modified duplex) - T_m(Control)

Table 2: Thermal and thermodynamic parameters from Differential Scanning Calorimetry

	-ΔH *Kcal/mol*		*-ΔS* *eu*		*-ΔG$_{37℃}$* *Kcal/mol*		*T$_m$*[b] *℃*		*ΔΔH*[C] Kcal/ mol	*ΔΔS*[d] eu	*ΔΔG$^{e}_{37℃}$* Kcal/mol	*ΔT$_m$*[f] ℃
	Um	Mod	Um	Mod	Um	Mod	Um	Mod				
Full duplex	115.7	101.8	320.8	287.0	16.3	12.8	66.8	58.8	13.9	33.8	3.5	-8.0
-3 deletion	76.9	73.4	214.6	206.2	10.3	9.5	54.9	51.8	3.5	8.4	0.8	-3.1
-2 deletion	88.3	97.9	254.1	274.1	9.5	13.0	49.4	60.2	-9.6	-20.0	-3.5	10.8
'AT' -1 deletion	99.6	121.5	284.7	335.5	11.3	17.6	54.0	69.2	-21.9	-50.8	-6.3	15.2
'GC' -1 deletion	90.3	105.5	250.0	281.0	12.8	18.4	61.7	77.7	-15.2	-31.0	-5.6	16.0

Blue: Unmodified, Red: Modified

a) The average standard deviation for –ΔG, -ΔH and T_m[b] are ± 0.4, ± 3.0 and ± 0.4 respectively.
b) T_m value is the temperature at half the peak area.
c) ΔΔH = ΔH(modified duplex) - ΔH(Control)
d) ΔΔS = ΔS(modified duplex) - ΔS(Control)
e) $\Delta\Delta G_{37℃}$ = ΔG(modified duplex) - ΔG(Control)
f) $\Delta T_m = T_m$ (modified duplex) - T_m(Control)

Table 3: Shifts in Wavelength of FAAF modified duplexes with respective control DNA duplexes

	Unmodified (G) Wavelength (nm)	**FAAF modified (G*) Wavelength (nm)**	**Shift in wavelength (nm) (Δ_{G-G*})**	**Type of Shift**
Full duplex	275 nm	270 nm	5 nm	Blue shift
-3 deltion	270 nm	273 nm	-3 nm	Red shift
-2 deletion	275 nm	272 nm	3 nm	Blue shift
'AT' -1 deletion	275 nm	271 nm	4 nm	Blue shift
'GC' -1 deletion	275 nm	271 nm	4 nm	Blue shift

G: Unmodified duplexes wavelength

G*: FAAF modified duplexes wavelength

Table 4: Shifts in wavelength of FAAF modified duplexes with respective to full unmodified duplex

	Wavelength (nm)	**Shift in wavelength (nm) (Δ_{G-G^*})**	**Type of Shift**
Control	275 nm	-	-
Full duplex	270 nm	5 nm	Blue shift
-3 deletion	273 nm	2 nm	Blue shift
-2 deletion	273 nm	2 nm	Blue shift
'AT' -1 deletion	271 nm	4 nm	Blue shift

G: Full Unmodified duplex wavelength

G*: FAAF modified duplex wavelength

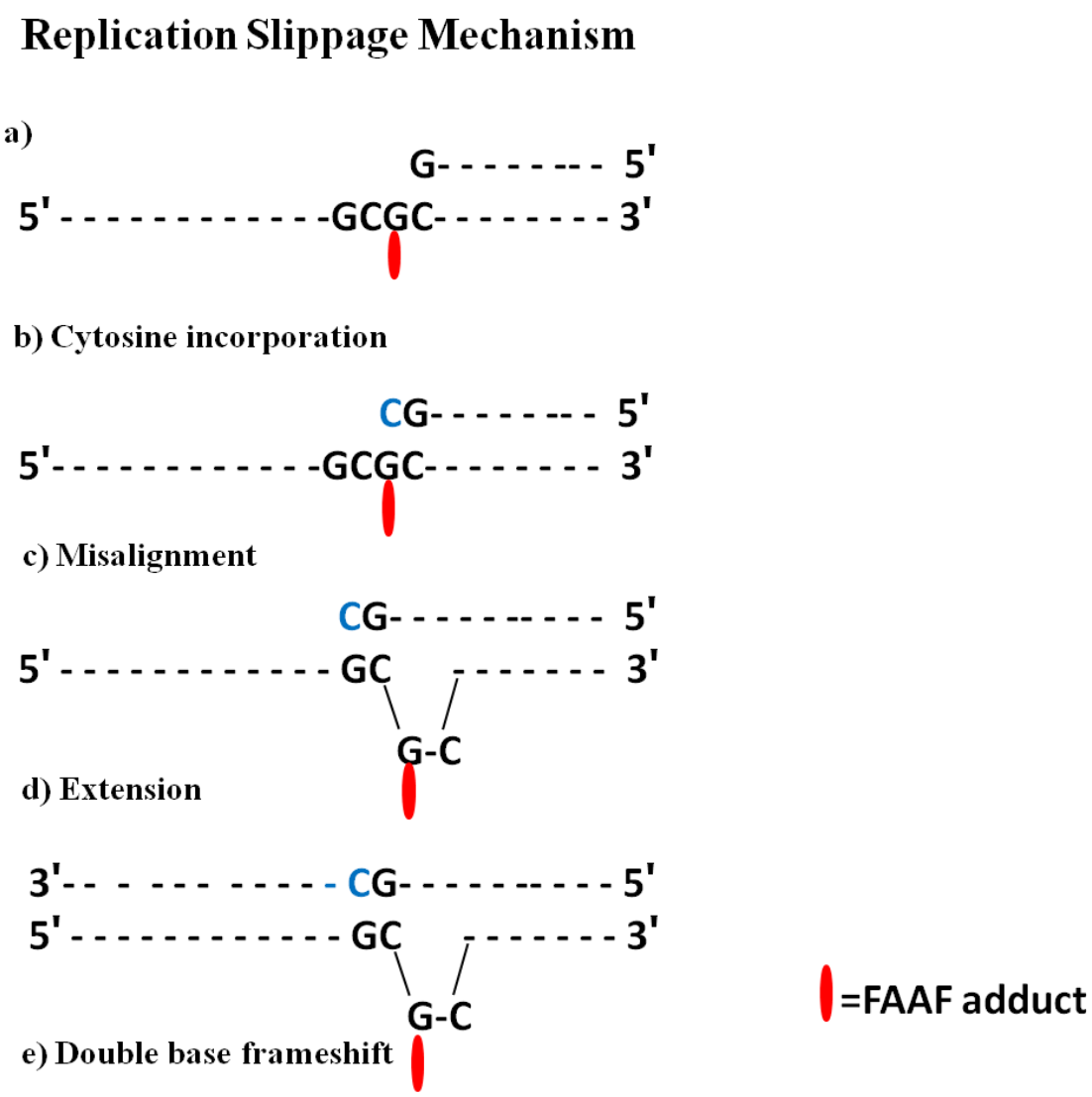

Figure 1: Reaction Slippage Mechanism of double base frameshift mutagenesis in *Nar*I sequence.

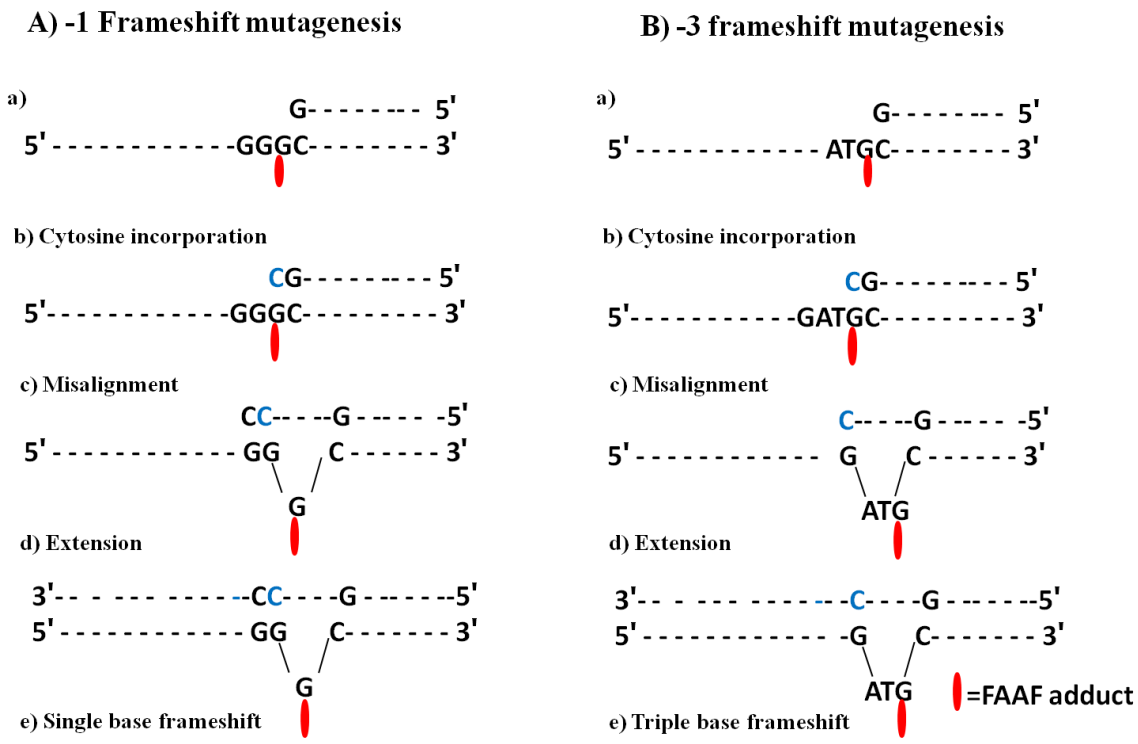

Figure 2: Reaction Slippage Mechanism of A) Single base frameshift mutagenesis B) -3 frameshift mutagenesis.

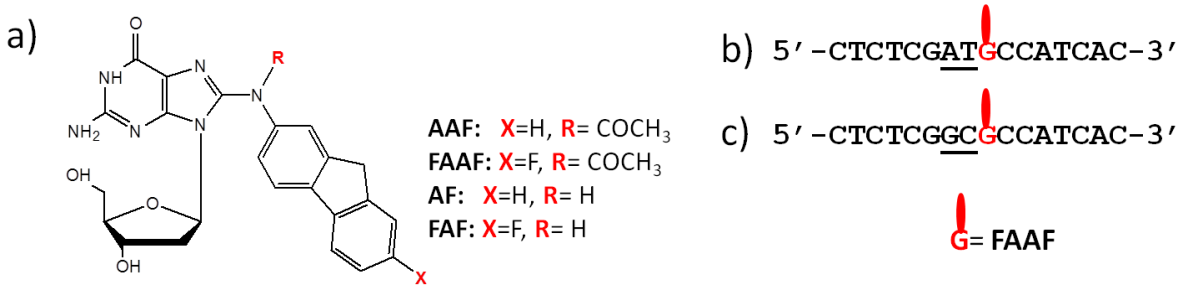

Figure 3: Structures and sequences used in this study. (a) Chemical structures of AAF, FAAF, AF, FAF sequence and (c) 16-mer *Nar*I sequences used in the present study.

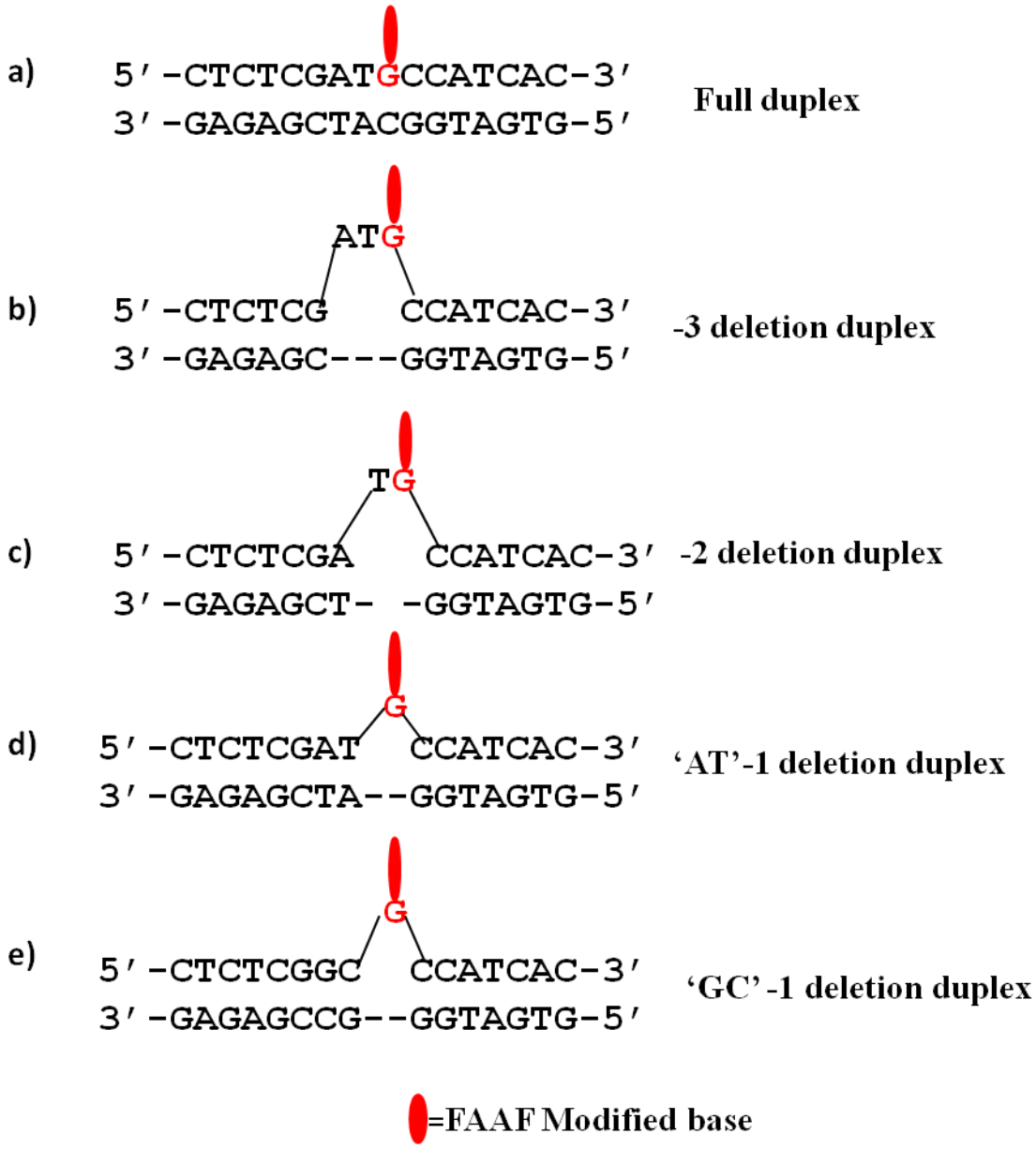

Figure 4: Model duplexes studied in the present study (a) Full duplex (b) -3 deletion duplex (c) -2 deletion duplex (d) 'AT' -1 deletion duplex (e) 'GC' -1 deletion duplex

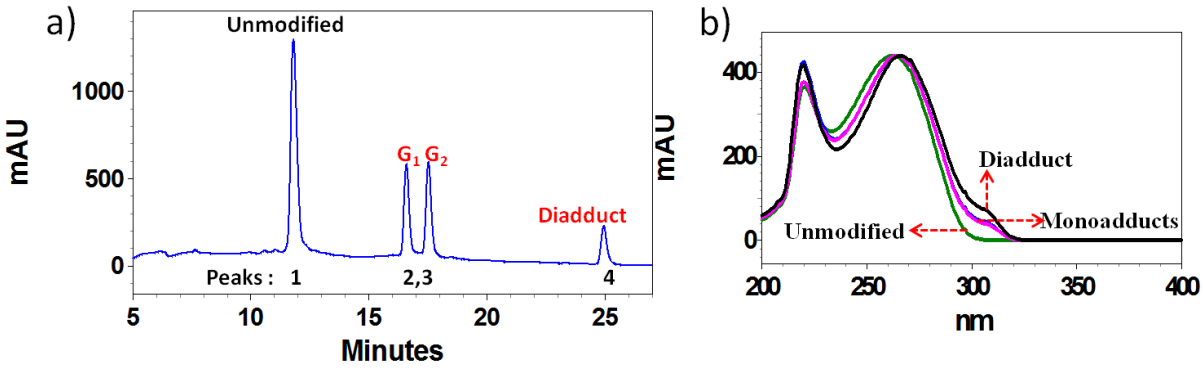

Figure 5: HPLC profile of FAAF-modified ODN. (a) Chromatogram of a reaction mixture between 16-mer sequence (5'-CTCTCG$_1$ATG$_2$CCATCAC-3') and an activated FAAF (N-acetoxy-N-2-(acetylamino)-7-fluorofluorene). The mono- (G_1, G_2) and di-FAAF adducts eluted in the 15-20, and 25 min ranges were purified by reversed-phase HPLC (see materials and method for gradient condition). (b) on-line photodiode array UV/Vis spectra of Unmodified, mono-, and di- FAAF adducts

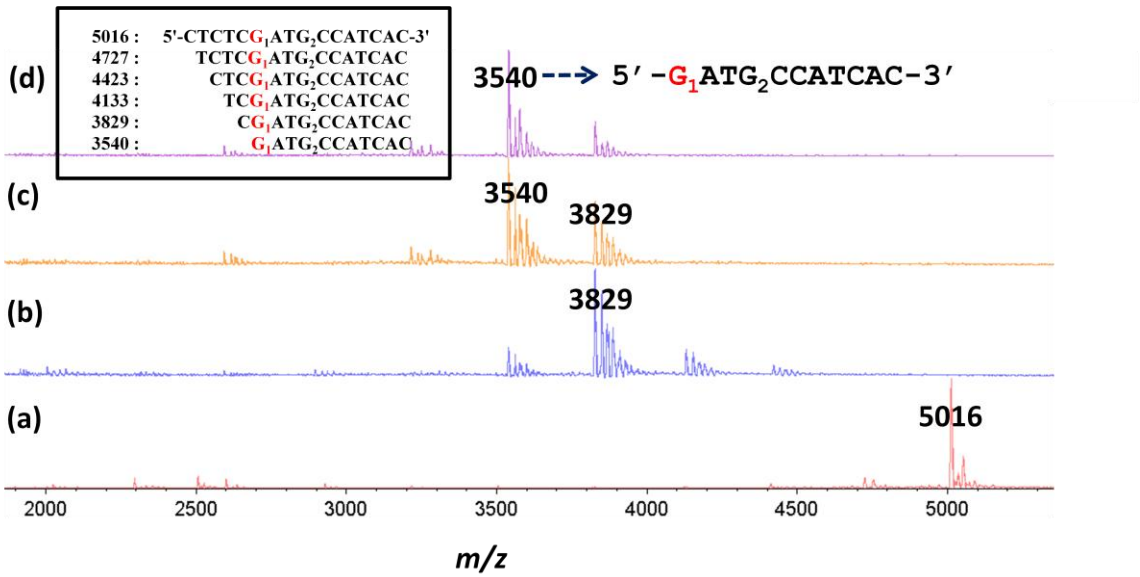

Figure 6: MALDI mass spectra of a of Peak 2 obtained from FAAF-modification of 16-mer template (5'-CTCTCG$_1$ATG$_2$CCATCAC-3') after 5'→3'exonuclease digestion using BSP enzyme conducted on MALDI-TOF-mass spectrometer in Reflectron mode at various time intervals (a) control (b) 15min (c) 45min (d) 60min.

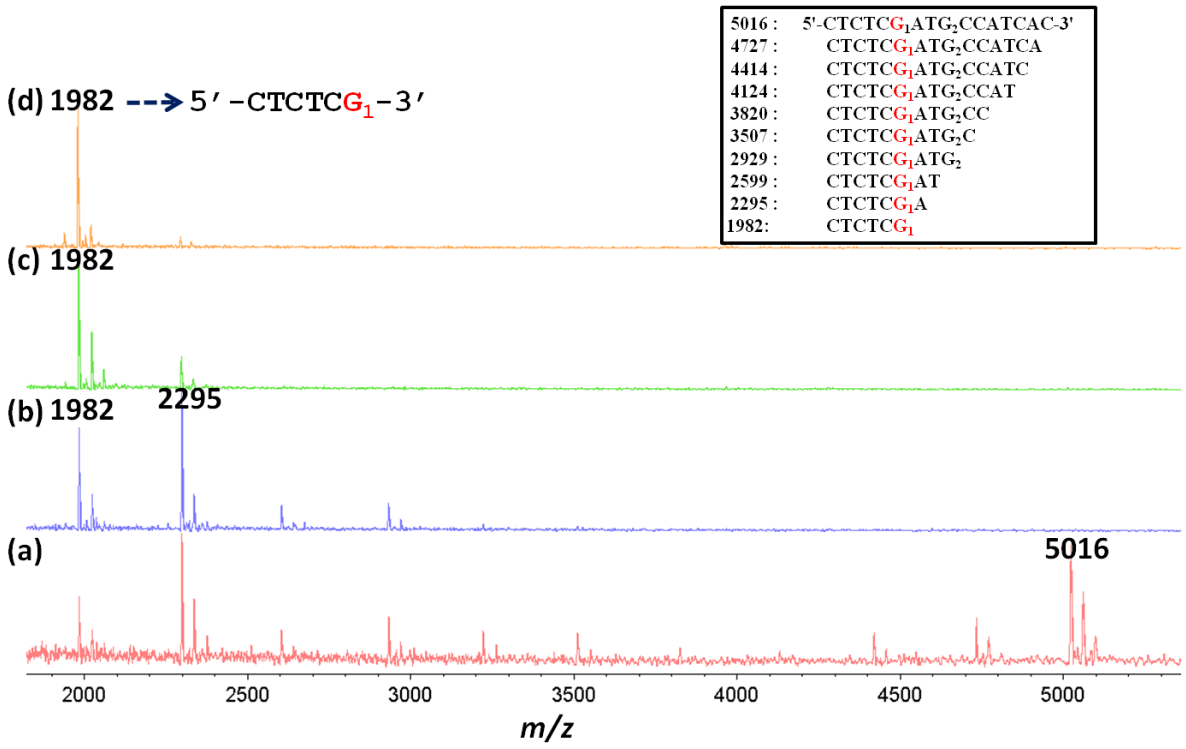

Figure 7: MALDI mass spectra of a of Peak 2obtained from FAAF-modification of 16-mer template (5'-CTCTCG$_1$ATG$_2$CCATCAC-3') after 3'→5'exonuclease digestion using SVP enzyme conducted on MALDI-TOF-mass spectrometer in Reflectron mode at various time intervals (a) control (b) 30sec (c) 2min (d) 5min .

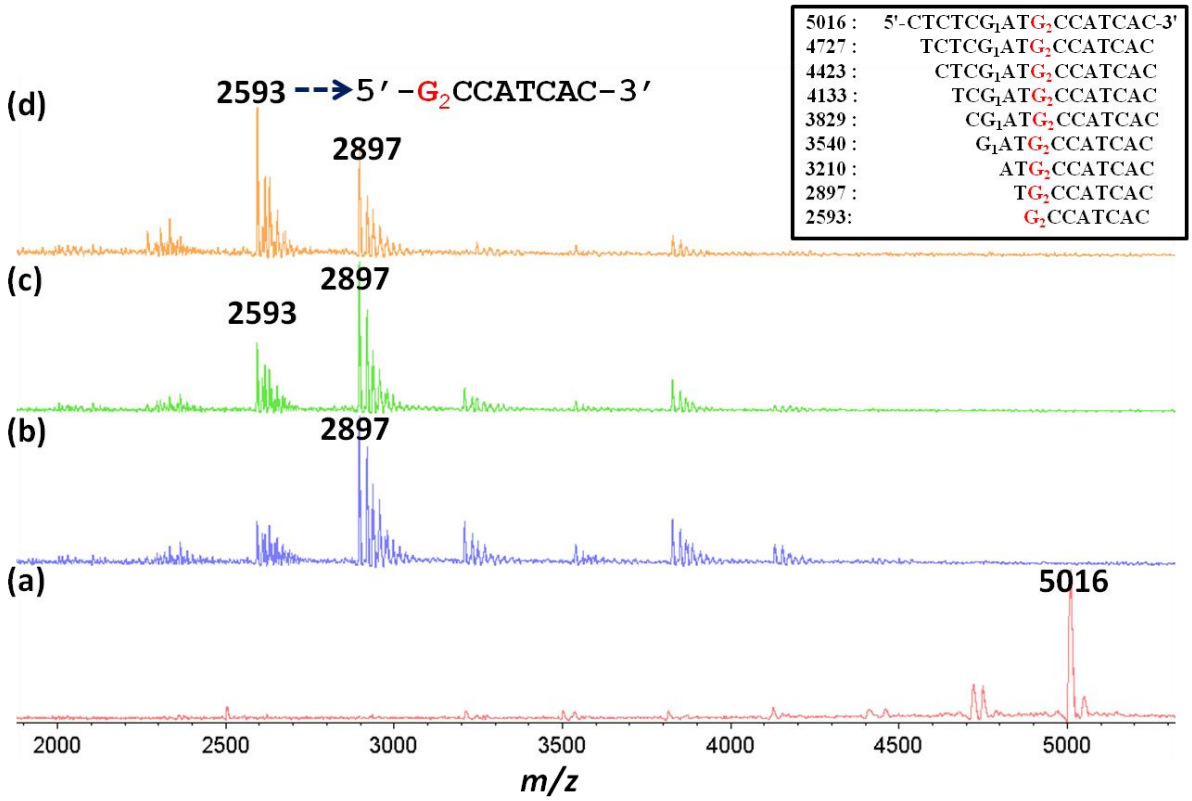

Figure 8: MALDI mass spectra of a of Peak 3 obtained from FAAF-modification of 16-mer template (5'-CTCTCG$_1$ATG$_2$CCATCAC-3') after 5'→3'exonuclease digestion using BSP enzyme conducted on MALDI-TOF-mass spectrometer in Reflectron mode at various time intervals (a) control (b) 15min (c) 45min (d) 60min.

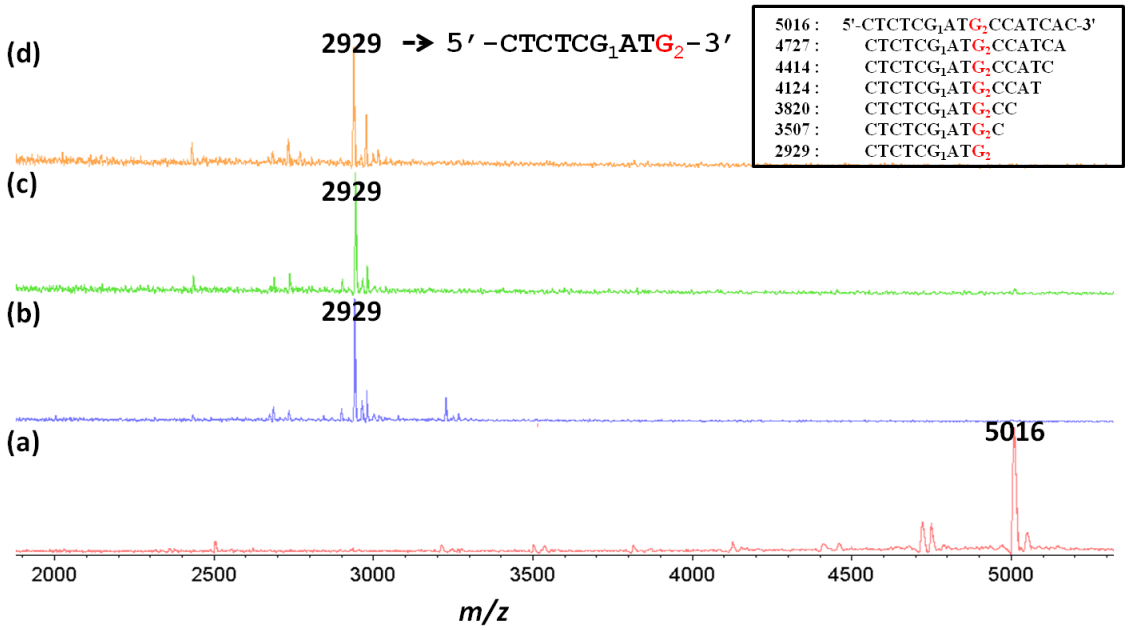

Figure 9: MALDI mass spectra of a of Peak 3obtained from FAAF-modification of 16-mer template (5'-CTCTCG$_1$ATG$_2$CCATCAC-3') after 3'→5'exonuclease digestion using SVP enzyme conducted on MALDI-TOF-mass spectrometer in Reflectron mode at various time intervals (a) control (b) 30sec (c) 2min (d) 5min .

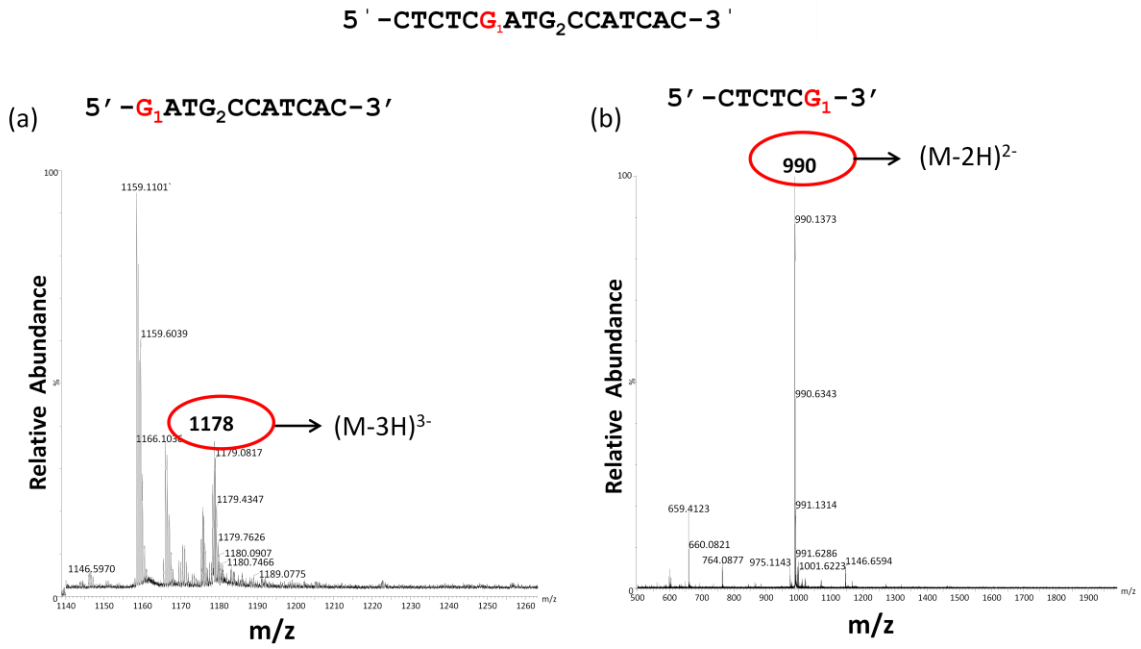

Figure 10: Molecular ion spectra of peak 2 obtained from FAAF-modification of (5'-$CTCTCG_1ATG_2CCATCAC$-3')16-mer template after (a) 5'-exonuclease digestion (b) 3'-exonuclease digestion conducted on Waters SYNAPT ESI-QTOF-mass spectrometer in negative ion and V-modes.

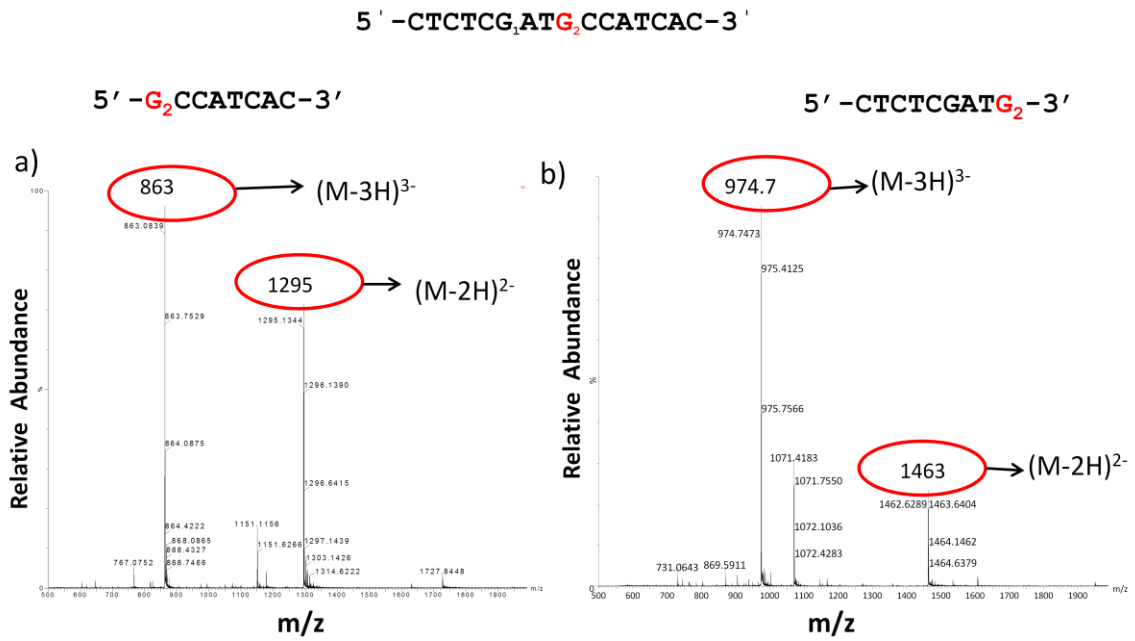

Figure 11: Molecular ion spectra of peak 3 obtained from FAAF-modification of (5'-CTCTCG$_1$ATG$_2$CCATCAC-3')16-mer template after a) 5'-exonuclease digestion b) 3'-exonuclease digestion conducted on Waters SYNAPT ESI-QTOF-mass spectrometer in negative ion and V-modes.

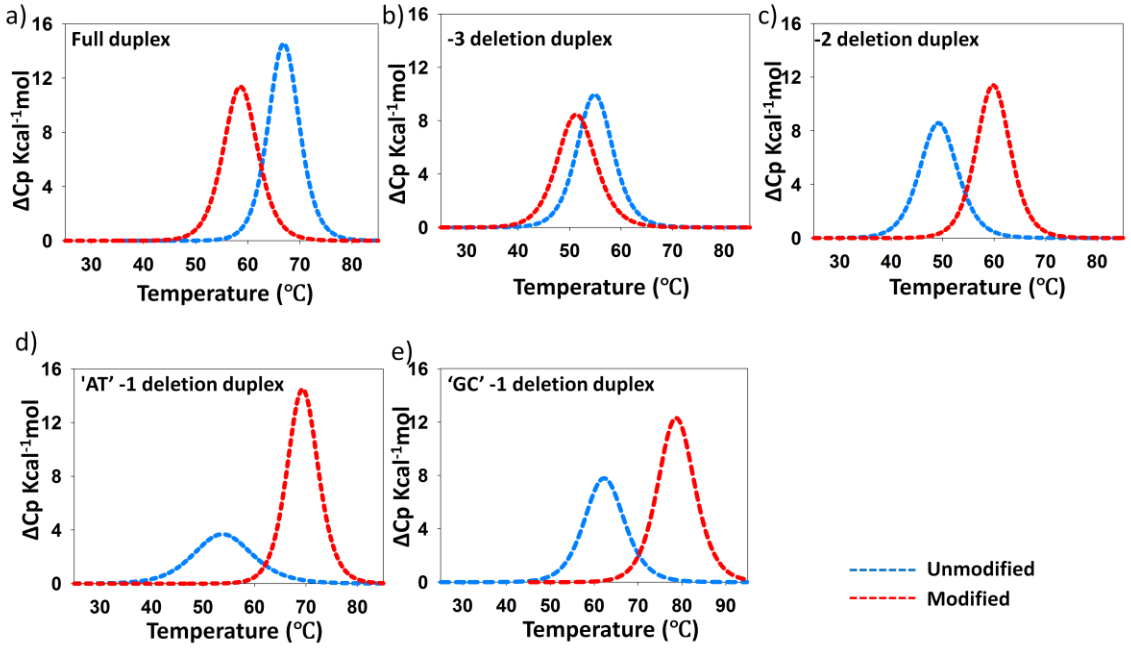

Figure 12: UV-melting curves of the five FAAF modified duplexes (Red) and respective unmodified control duplex, (blue) all at 10μM in 0.2 M NaCl, 10 mM sodium phosphate, and 0.2 mM EDTA at pH 7 a) Full duplex b) -3 deletion duplex c) -2 deletion duplex d) 'AT'-1 deletion duplex e) 'GC' -1 deletion duplex

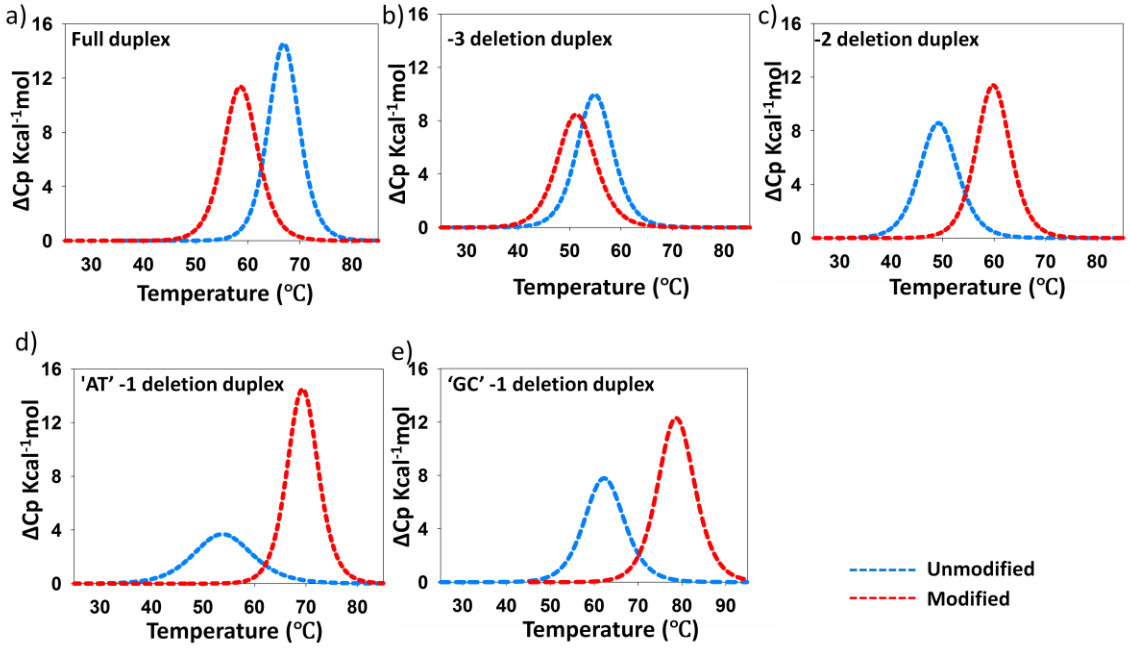

Figure 13: Differential scanning calorimetry (DSC) curves in 20 mM phosphate buffer containing 0.1 M NaCl at pH 7 of a) Full duplex b)-3 deletion duplex c) -2 deletion duplex d) -1 deletion duplex e) 'GC' -1 deletion duplex with FAAF modified duplexes indicated in Red and Unmodified duplexes in blue.

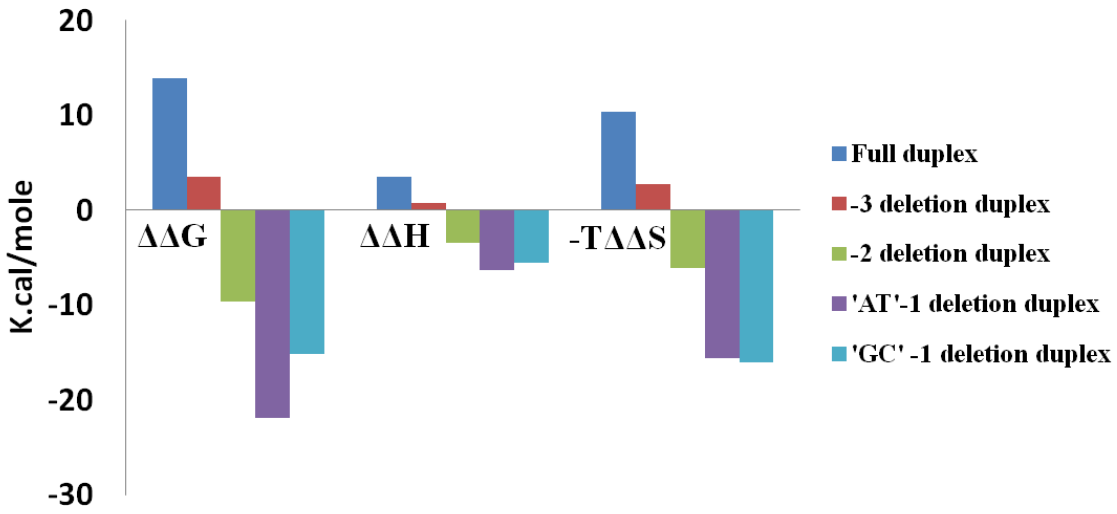

Figure 14: Thermodynamic plots of the FAAF- modified duplexes with respective to their unmodified duplex.

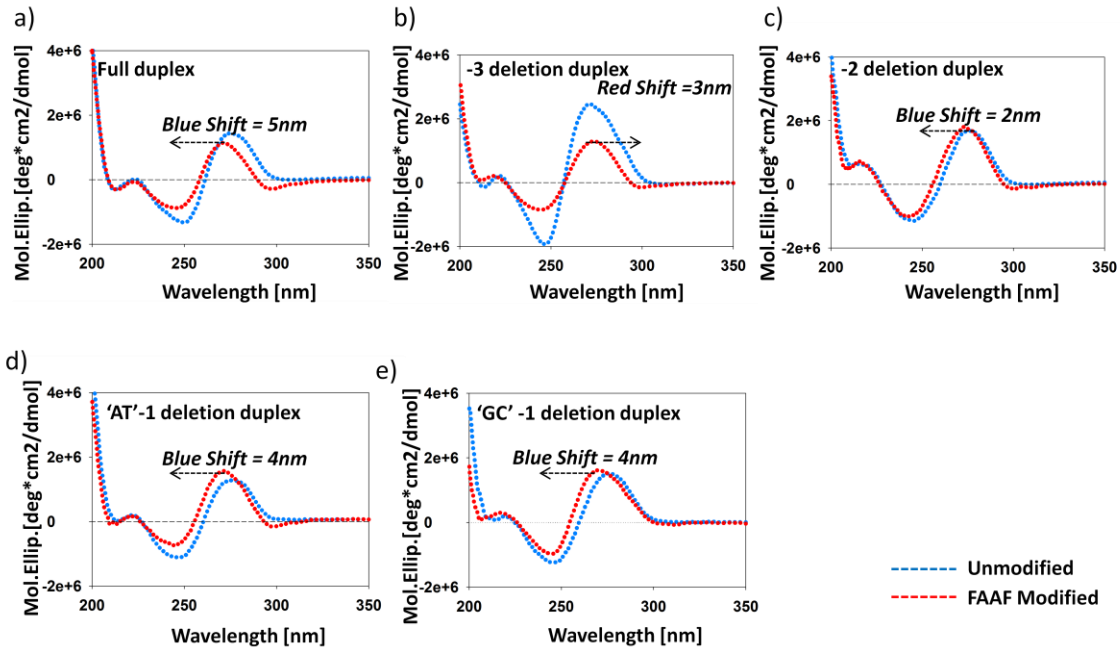

Figure 15: CD Spectral overlay recorded at 30 °C of (a) Full duplex (b)-3 deletion duplex (c) -2 deletion duplex (d) 'AT' -1 deletion duplex (e) 'GC' -1 deletion duplex with FAAF modified duplexes indicated in Red and unmodified duplexes in blue.

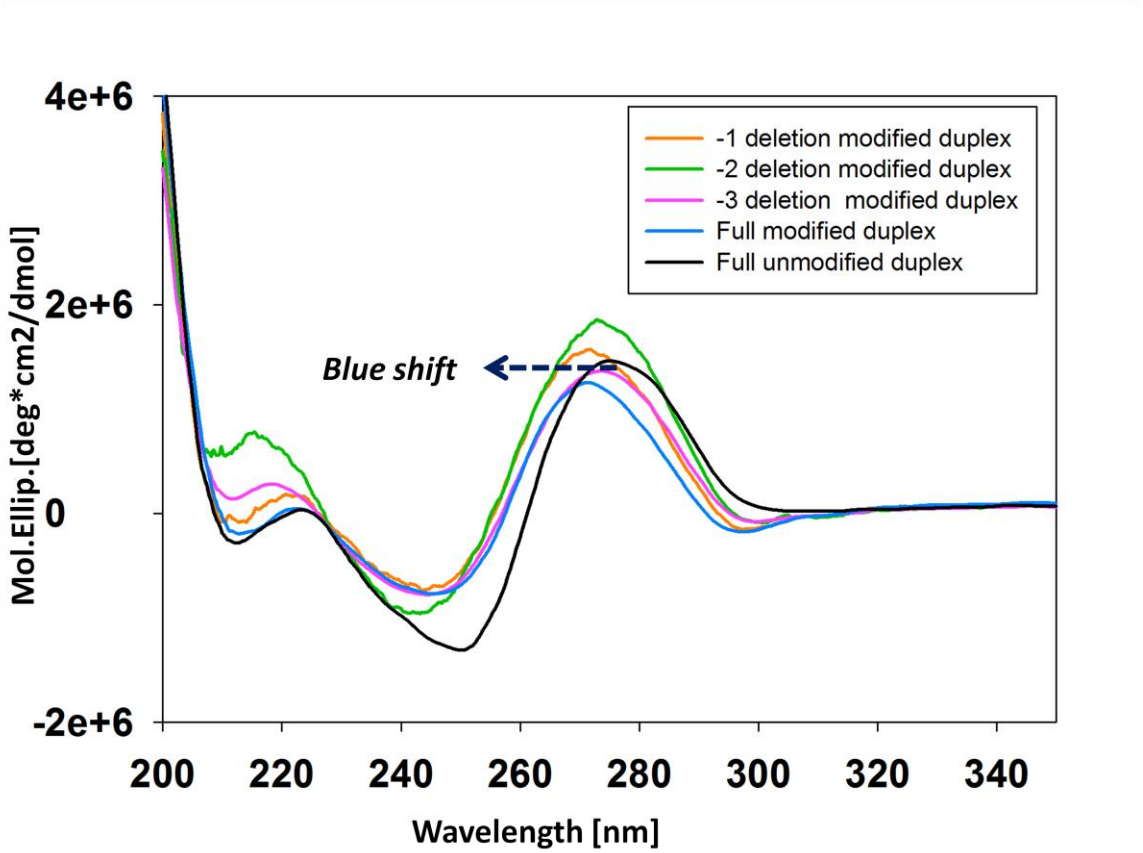

Figure 16: CD Spectral overlay recorded at 30 °C of FAAF modified (a) Full duplex (b)-3 deletion duplex (c) -2 deletion duplex (d) 'AT' -1 deletion duplex with respective to full unmodified duplex (control).

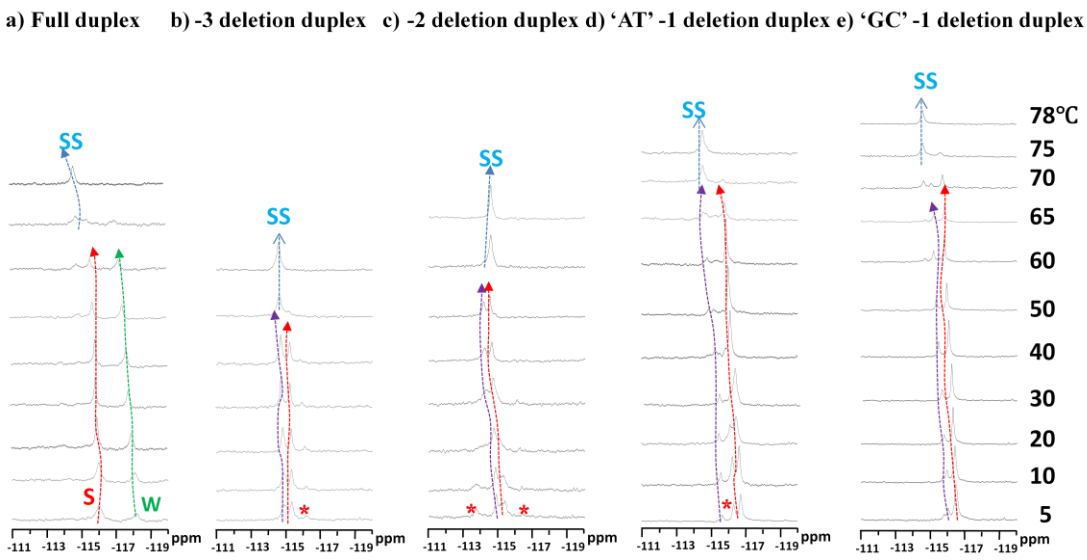

Figure 17: Dynamic ^{19}F NMR spectra of FAAF modified a) Full duplex b)-3 deletion duplex c) -2 deletion duplex d) 'AT'-1 deletion duplex e) 'GC' -1 deletion duplex

------ External conformation

------Stacked conformation

------Wedged conformation

------Single strand

*** Unknown Conformation**

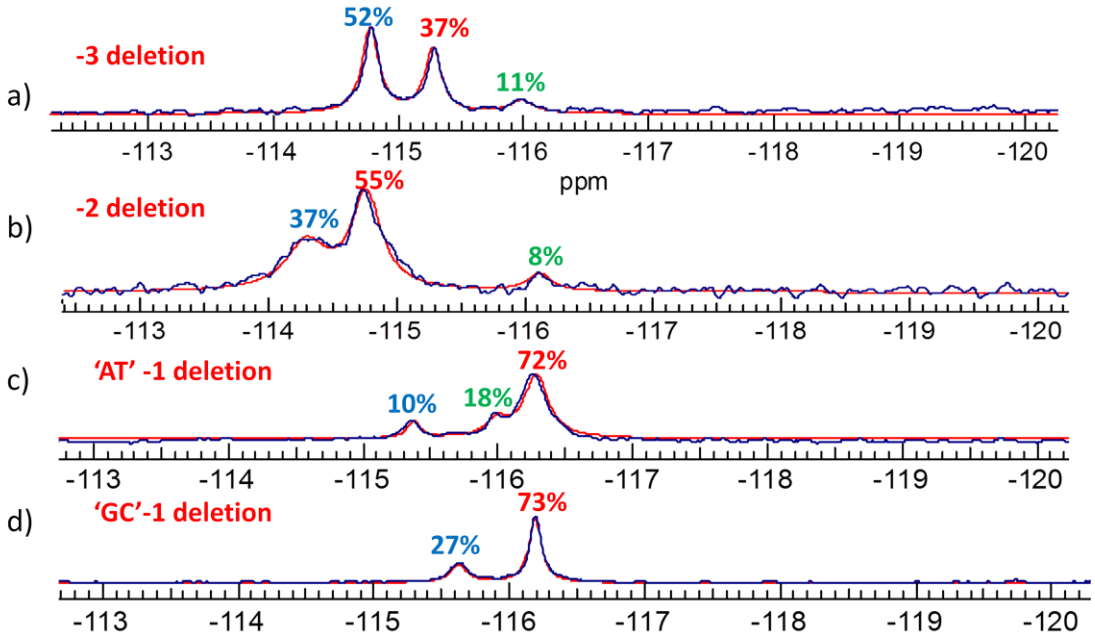

Figure 18: Line simulation of FAAF-modified 16-mer (5'-CTCTCG$_1$<u>AT</u>G$_2$CCATCAC-3') (a) -3 deletion (b) -2 deletion (c) 'AT'-1 deletion duplexes and FAAF modified *Nar*I 16-mer (5'-CTCTCG$_1$<u>GC</u>G$_3$CCATCAC-3') (e) GC' -1 deletion duplex at 30 ˚C.

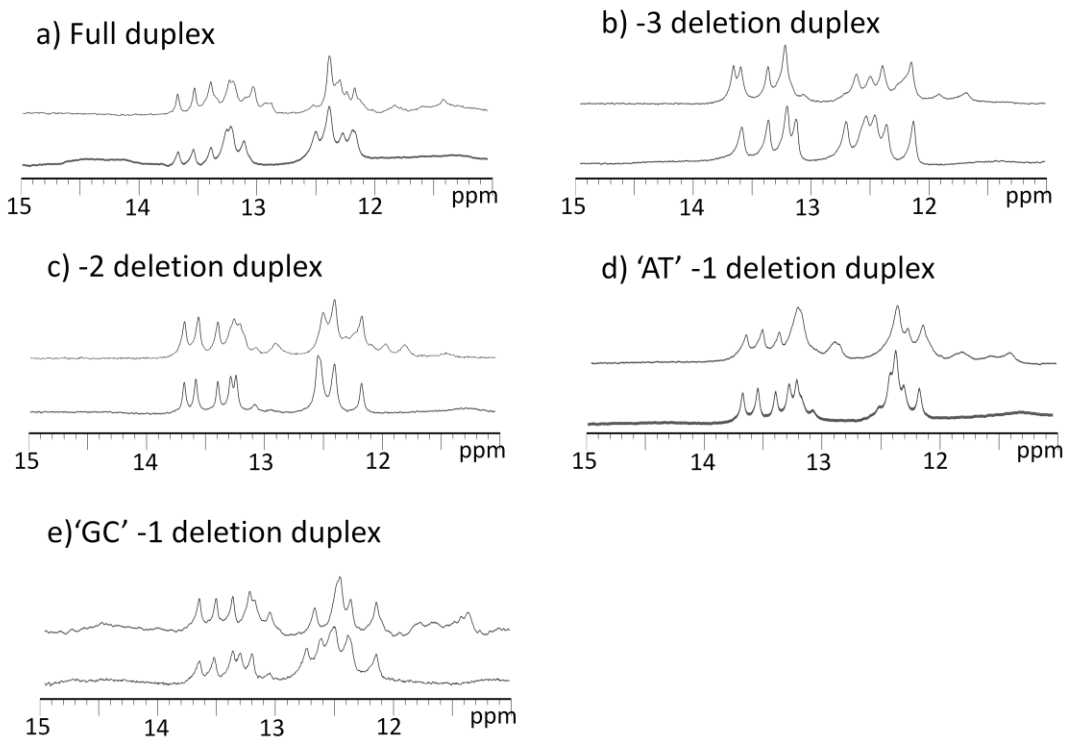

Figure 19: Imino proton region (11-15 ppm) of proton NMR of FAAF-modified 16-mer (5'-CTCTCG$_1$<u>AT</u>G$_2$CCATCAC-3') (a) Full duplex (b) -3 deletion (c) -2 deletion (d) 'AT' -1 deletion duplexes and FAAF modified *Nar* I 16-mer (5'-CTCTCG$_1$<u>G$_2$C</u>G$_3$CCATCAC-3') (e) 'GC' -1 deletion duplex with respective to the unmodified duplexes at 5˚C.

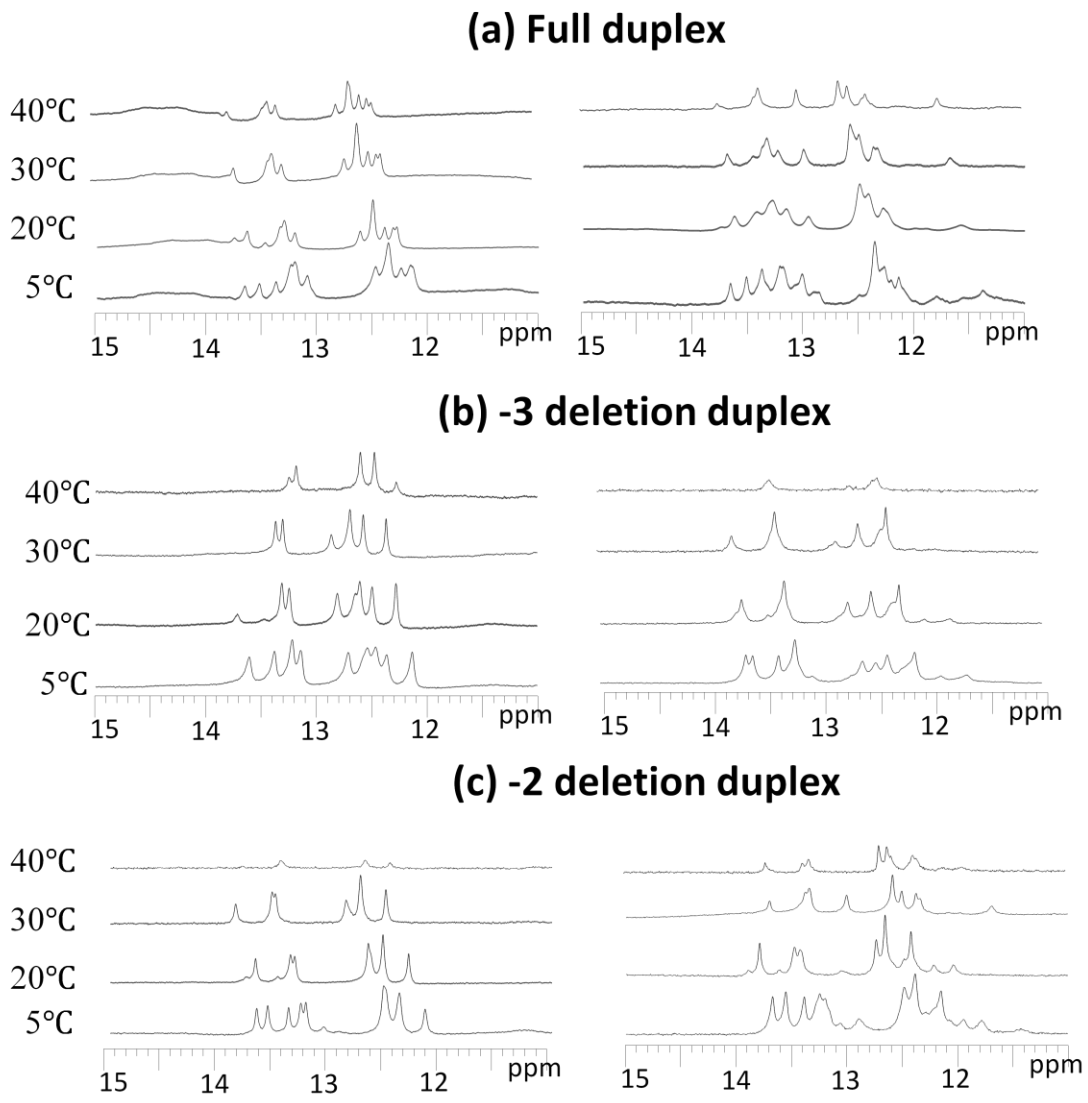

Figure 20: Imino proton region (11-15 ppm) of proton NMR of FAAF-modified 16-mer (5ˈ-CTCTCG$_1$<u>AT</u>G$_2$CCATCAC-3ˈ) (a) Full duplex (b) -3 deletion (c) -2 deletion duplex with respective to the unmodified duplexes at 5,20,30,40˚C.

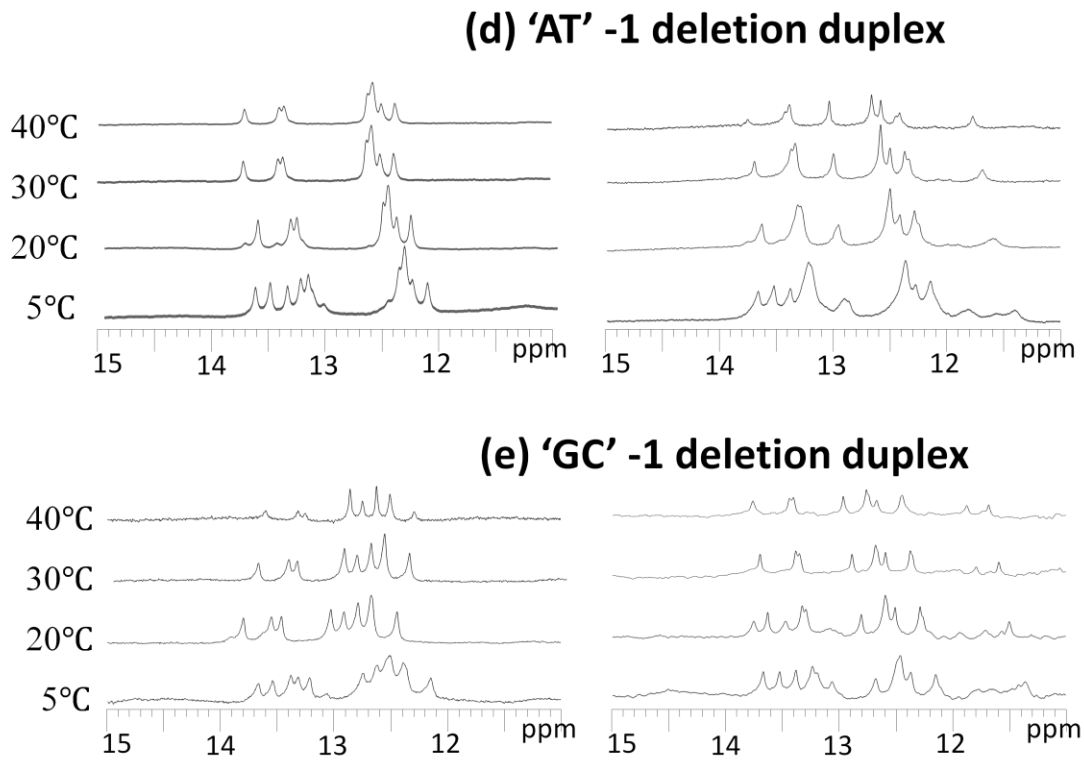

Figure 21: Imino proton region (11-15 ppm) of proton NMR of FAAF-modified 16-mer (5'-CTCTCG$_1$<u>AT</u>G$_2$CCATCAC-3') (d) 'AT' -1 deletion duplexes and FAAF modified *Nar* I 16-mer (5'-CTCTCG$_1$<u>G$_2$C</u>G$_3$CCATCAC-3') (e) 'GC' -1 deletion duplex with respective to the unmodified duplexes at 5,20,30,40˚C.

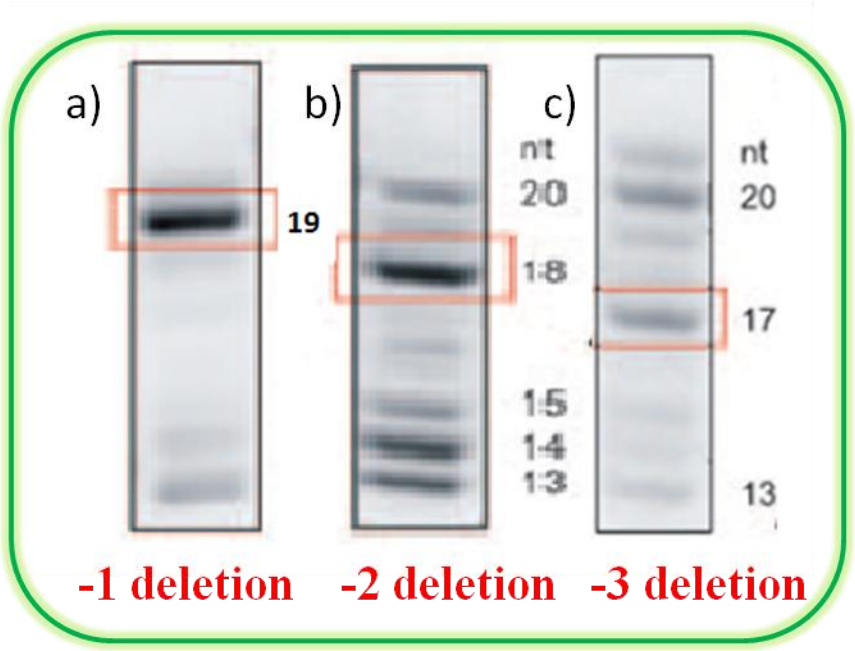

Figure 22: Comparison of primer extension assay products by gel electrophoresis a) -1 deletion b)-2 deletion c) -3 deletion (S. Schorr and T. Carell; *ChemBioChem, 2010, 2534)*

List of References:

1. Luch, A. (2005) Nature and nurture - lessons from chemical carcinogenesis, *Nat Rev Cancer 5*, 113-125.
2. Heflich, R. H., and Neft, R. E. (1994) Genetic toxicity of 2-acetylaminofluorene, 2-aminofluorene and some of their metabolites and model metabolites, *Mutation Research/Reviews in Genetic Toxicology 318*, 73-174.
3. Hoffmann, G. R., and Fuchs, R. P. P. (1997) Mechanisms of Frameshift Mutations: Insight from Aromatic Amines, *Chemical Research in Toxicology 10*, 347-359.
4. Beland, F. A., and Kadlubar, F. F. (1990) *Handbook of Experimental Pharmacology*, Spring-Verlag, Heidelberg.
5. Shibutani, S., Suzuki, N., Tan, X., Johnson, F., and Grollman, A. P. (2001) Influence of Flanking Sequence Context on the Mutagenicity of Acetylaminofluorene-Derived DNA Adducts in Mammalian Cells, *Biochemistry 40*, 3717-3722.
6. Belguise-Valladier, P., and Fuchs, R. P. P. (1991) *Biochemistry 30*, 10091.
7. Ames, B. N., Gurney, E. G., Miller, J. A., and Bartsch, H. (1972) Carcinogens as frameshift mutagens: metabolites and derivatives of 2-acetylaminofluorene and other aromatic amine carcinogens, *Proc Natl Acad Sci U S A 69*, 3128-3132.
8. Zhang, Y., Yuan, F., Wu, X., Rechkoblit, O., Taylor, J. S., Geacintov, N. E., and Wang, Z. (2000) Error-prone lesion bypass by human DNA polymerase eta, *Nucleic Acids Res 28*, 4717-4724.

9. Ohmori, H., Friedberg, E. C., Fuchs, R. P., Goodman, M. F., Hanaoka, F., Hinkle, D., Kunkel, T. A., Lawrence, C. W., Livneh, Z., Nohmi, T., Prakash, L., Prakash, S., Todo, T., Walker, G. C., Wang, Z., and Woodgate, R. (2001) The Y-family of DNA polymerases, *Mol Cell 8*, 7-8.

10. Bresson, A., and Fuchs, R. P. (2002) Lesion bypass in yeast cells: Pol eta participates in a multi-DNA polymerase process, *EMBO J 21*, 3881-3887.

11. Hsu, G. W., Kiefer, J. R., Burnouf, D., Becherel, O. J., Fuchs, R. P. P., and Beese, L. S. (2004) Observing Translesion Synthesis of an Aromatic Amine DNA Adduct by a High-fidelity DNA Polymerase, *J. Biol. Chem. 279*, 50280-50285.

12. Fuchs, R. P., Schwartz, N., and Daune, M. P. (1981) Hot spots of frameshift mutations induced by the ultimate carcinogen N-acetoxy-N-2-acetylaminofluorene, *Nature 294*, 657-659.

13. Koffel-Schwartz, N., and Fuchs, R. P. (1995) Sequence determinants for -2 frameshift mutagenesis at NarI-derived hot spots, *J Mol Biol 252*, 507-513.

14. Fuchs, R. P., Koffel-Schwartz, N., Pelet, S., Janel-Bintz, R., Napolitano, R., Becherel, O. J., Broschard, T. H., Burnouf, D. Y., and Wagner, J. (2001) DNA polymerases II and V mediate respectively mutagenic (-2 frameshift) and error-free bypass of a single N-2-acetylaminofluorene adduct, *Biochem Soc Trans 29*, 191-195.

15. Fuchs, R. P., and Fujii, S. (2007) Translesion synthesis in Escherichia coli: lessons from the NarI mutation hot spot, *DNA Repair (Amst) 6*, 1032-1041.

16. Suzuki, N., Yasui, M., Santosh Laxmi, Y. R., Ohmori, H., Hanaoka, F., and Shibutani, S. (2004) Translesion synthesis past equine estrogen-derived 2'-

deoxycytidine DNA adducts by human DNA polymerases eta and kappa, *Biochemistry 43*, 11312-11320.

17. Koffel-Schwartz, N., Verdier, J. M., Bichara, M., Freund, A. M., Daune, M. P., and Fuchs, R. P. (1984) Carcinogen-induced mutation spectrum in wild-type, uvrA and umuC strains of Escherichia coli. Strain specificity and mutation-prone sequences, *J Mol Biol 177*, 33-51.
18. Hoffmann, G. R., and Fuchs, R. P. (1997) Mechanisms of frameshift mutations: insight from aromatic amines, *Chem Res Toxicol 10*, 347-359.
19. Roy, D., Hingerty, B. E., Shapiro, R., and Broyde, S. (1998) A slipped replication intermediate model is stabilized by the syn orientation of N-2-aminofluorene- and N-2-(acetyl)aminofluorene-modified guanine at a mutational hotspot, *Chem Res Toxicol 11*, 1301-1311.
20. Schorr, S., and Carell, T. (2010) Mechanism of acetylaminofluorene-dG induced frameshifting by polymerase eta, *Chembiochem 11*, 2534-2537.
21. O'Handley, S. F., Sanford, D. G., Xu, R., Lester, C. C., Hingerty, B. E., Broyde, S., and Krugh, T. R. (1993) Structural characterization of an N-acetyl-2-aminofluorene (AAF) modified DNA oligomer by NMR, energy minimization, and molecular dynamics, *Biochemistry 32*, 2481-2497.
22. Cho, B. P., and Zhou, L. (1999) Probing the conformational heterogeneity of the acetylaminofluorene-modified 2'-deoxyguanosine and DNA by 19F NMR spectroscopy, *Biochemistry 38*, 7572-7583.

23. Milhe, C., Dhalluin, C., Fuchs, R. P., and Lefevre, J. F. (1994) NMR evidence of the stabilisation by the carcinogen N-2-acetylaminofluorene of a frameshift mutagenesis intermediate, *Nucleic Acids Res 22*, 4646-4652.

24. Milhe, C., Fuchs, R. P., and Lefevre, J. F. (1996) NMR data show that the carcinogen N-2-acetylaminofluorene stabilises an intermediate of -2 frameshift mutagenesis in a region of high mutation frequency, *Eur J Biochem 235*, 120-127.

25. Mao, B., Cosman, M., Hingerty, B. E., Broyde, S., and Patel, D. J. (1995) Solution conformation of [AF]dG opposite a -1 deletion site in a DNA duplex: intercalation of the covalently attached aminofluorene ring into the helix with base displacement of the C8-modified Syn guanine into the major groove, *Biochemistry 34*, 6226-6238.

26. Mao, B., Gorin, A., Gu, Z., Hingerty, B. E., Broyde, S., and Patel, D. J. (1997) Solution structure of the aminofluorene-intercalated conformer of the syn [AF]-C8-dG adduct opposite a--2 deletion site in the NarI hot spot sequence context, *Biochemistry 36*, 14479-14490.

27. Cosman, M., Fiala, R., Hingerty, B. E., Amin, S., Geacintov, N. E., Broyde, S., and Patel, D. J. (1994) Solution conformation of the (+)-trans-anti-[BP]dG adduct opposite a deletion site in a DNA duplex: intercalation of the covalently attached benzo[a]pyrene into the helix with base displacement of the modified deoxyguanosine into the major groove, *Biochemistry 33*, 11507-11517.

28. Geacintov, N. E., Cosman, M., Hingerty, B. E., Amin, S., Broyde, S., and Patel, D. J. (1997) NMR solution structures of stereoisometric covalent polycyclic

aromatic carcinogen-DNA adduct: principles, patterns, and diversity, *Chem Res Toxicol 10*, 111-146.

30. Patnaik, S., and Cho, B. P. (2010) Structures of 2-acetylaminofluorene modified DNA revisited: insight into conformational heterogeneity, *Chem Res Toxicol 23*, 1650-1652.

31. Gao, L., Zhang, L., Cho, B., and Chiarelli, M. (2008) Sequence verification of oligonucleotides containing multiple arylamine modifications by enzymatic digestion and liquid chromatography mass spectrometry (LC/MS), *Journal of the American Society for Mass Spectrometry 19*, 1147-1155.

32. Meneni, S. R., D'Mello, R., Norigian, G., Baker, G., Gao, L., Chiarelli, M. P., and Cho, B. P. (2006) Sequence effects of aminofluorene-modified DNA duplexes: thermodynamic and circular dichroism properties, *Nucleic Acids Res 34*, 755-763.

33. Zhou, L., Rajabzadeh, M., Traficante, D. D., and Cho, B. P. (1997) Conformational Heterogeneity of Arylamine-Modified DNA: 19F NMR Evidence, *J Am Chem Soc 119*, 5384-5389.

34. Jain, N., Li, Y., Zhang, L., Meneni, S. R., and Cho, B. P. (2007) Probing the sequence effects on NarI-induced -2 frameshift mutagenesis by dynamic 19F NMR, UV, and CD spectroscopy, *Biochemistry 46*, 13310-13321.

35. Jain, N., Meneni, S., Jain, V., and Cho, B. P. (2009) Influence of flanking sequence context on the conformational flexibility of aminofluorene-modified dG adduct in dA mismatch DNA duplexes, *Nucleic Acids Res 37*, 1628-1637.

36. Meneni, S. R., Shell, S. M., Gao, L., Jurecka, P., Lee, W., Sponer, J., Zou, Y., Chiarelli, M. P., and Cho, B. P. (2007) *Biochemistry 46*, 11263.

37. Chakrabarti, M. C., and Schwarz, F. P. (1999) Thermal stability of PNA/DNA and DNA/DNA duplexes by differential scanning calorimetry, *Nucleic Acids Res 27*, 4801-4806.

38. Jain, V., Hilton, B., Patnaik, S., Zou, Y., Chiarelli, M. P., and Cho, B. P.(2012) Conformational and thermodynamic properties modulate the nucleotide excision repair of 2-aminofluorene and 2-acetylaminofluorene dG adducts in the NarI sequence, *Nucleic Acids Res 40*, 3939-3951.

39. Liang, F., and Cho, B. P. (2010) Enthalpy-entropy contribution to carcinogen-induced DNA conformational heterogeneity, *Biochemistry 49*, 259-266.

40. Jain, V., Hilton, B., Patnaik, S., Zou, Y., Chiarelli, M. P., and Cho, B. P. (2012) Conformational and thermodynamic properties modulate the nucleotide excision repair of 2-aminofluorene and 2-acetylaminofluorene dG adducts in the NarI sequence, *Nucleic Acids Res 40*, 3939-3951.

41. GD, F. (1996) *Circular Dichroism and the Conformational analysis of Biomolecules (Plenum press).*

42. Schaaper, R. M., Koffel-Schwartz, N., and Fuchs, R. P. P. (1990) N-acetoxy-N-acetyl-2-aminofluorene-induced mutagenesis in the lacI gene of Escherichia coli., *Carcinogenesis 11*, 1087.

Addendum

Description of various biophysical techniques used in this thesis work

UV-Melting experiments:

UV melting is used for determining the thermal and thermodynamic stability of DNA duplexes. The technique requires relative small amount (1-10 □M range) of oligonucleotide samples compare to other methods (DSC and NMR see below). UV absorption at 260 nm increases when a DNA duplex in solution is heated above its melting temperature, i.e., a double-stranded DNA unwinds to two separate single-stranded DNA. As a result, the bases become unstacked and can thus absorb more light ("hyperchromic" effect). Upon cooling, however, the bases become stacked, resulting in less absorption ("hypochromic" effect).

A graph of UV absorbance at 260 nm (*A*) against temperature (*T*) of a typical DNA duplex gives a characteristic sigmoidal curve. The mid-point of the melting curve is called "melting temperature," or T_m. T_m is an indication of DNA duplex stability, and can be used to determine thermodynamic parameters for melting. Typically, UV absorbances of a DNA sample having different concentrations are measured at 260 nm. The samples are heated between 15-90 °C with a heating rate of 10°C /min. A reverse scan is also performed on the same samples, by measuring the absorbencies from 90°C to 15°C. Usually a total of six melting curves are obtained by repeating the forward-reverse cycles three times. The UV melting data is then exported to the simulation software Meltwin (version 3.5) to determine various thermodynamic parameters based on a bimolecular melting process. The thermodynamic parameters such as enthalpy ($-\Delta H^0$), entropy ($-\Delta S^0$)

and Gibb's free energy ($-\Delta G^0$) of duplex-single strand equilibrium and melting temperature (T_m) are derived from the absorbance data and also from the melting curves. For this purpose two different methods are used: namely, curve fit and a plot of T_m^{-1} vs lnCt using van't Hoff equation $T_m^{-1} = R/\Delta H^0 \ lnCt/4 + \Delta S^0/\Delta H^0$. Standard thermodynamic equation $\Delta G^0 = \Delta H^0 - T\Delta S^0$ is used for calculation of ΔG^0. Tm is a melting transition point measured in Kelvin and R is the universal gas constant.

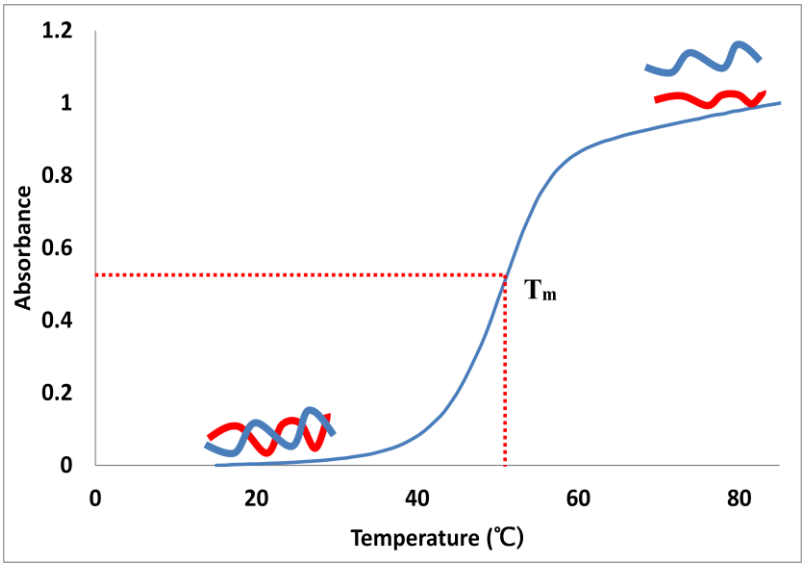

Differential Scanning Calorimetry (DSC)

DSC is a micro calorimetry technique and measures the changes in heat capacity (ΔC_p) as a function of temperature. DSC is considered be more reliable than UV-Melting because it is system independent. Typically, about 0.1 mM of the duplex sample is used in the sample cell and is scanned against buffer from 15 °C to 90 °C at a rate of 0.75°C/min. Raw data are collected as microwatts vs. temperature. At least five repetitions are obtained. A buffer vs. buffer scan is used as a control and subtracted from the sample

scan and normalized for heating rate. This result in base-corrected ΔC_p^{ex} (Kcal.mol^{-1}.K^{-1}) versus temperature (°C) curves, an example of DSC melting curve is shown below. Each transition shows negligible changes in the heat capacities between the initial and final states, thus assumed to be zero. The area of the resulting curve is proportional to the transition heat, which, when normalized for the number of moles of the sample, is equal to the transition enthalpy, ΔH. ΔH is an integration of ΔC_p^{ex} over temperature T. T_m is obtained from the mid temperature point of the bell shaped curve. T_m is defined as the mid temperature point of the double-strands to single strands. ΔG and ΔS values are determined from ΔH and T_m values. Based on these values Thermal and Thermodynamic stability of various deletion duplexes were found.

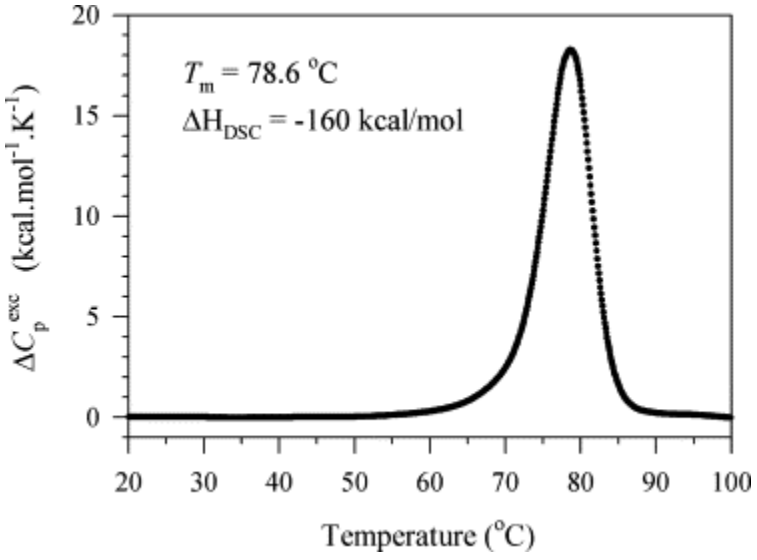

^{19}F NMR Spectroscopy

The sensitivity of the ^{19}F nucleus to the macromolecular environment and the lack of background noise in dealing with complex conformations votes to opt this technique.

^{19}F NMR spectroscopy is an excellent tool to probe into the conformational heterogeneity of modified DNA and proteins. The fluorine technique was used in my thesis to analyze DNA-adduct conformation in various deletion DNA duplexes. ^{19}F act as a probe to determine the position of lesion in bulged duplexes. ^{19}F NMR spectra were acquired in the ^{1}H-decoupled mode and referenced relative to that of $CFCl_3$ by assigning external C_6F_6 in C_6D_6 at -164.9 ppm. ^{19}F NMR spectra were measured between 5 and 78°C with increment of 5-10°C. Temperatures were maintained by an FTS unit.

Usually ^{19}F-NMR spectra are obtained in a pH 7.0 aqueous NMR buffer in D_2O. For imino proton spectra, however, it is necessary to use a 10% D_2O/90% H_2O buffer, which prevents potential exchange of the imino protons involved in the Watson-Crick base pairs. Frequently, both ^{19}F- and imino NMR spectra are acquired at various temperatures in order to examine the adduct-induced heterogeneity around the lesion site and also to calculate the kinetic and thermodynamics parameters. Assignment of ^{19}F NMR signals is often difficult due to lack of related signals (i.e., NOE or scalar couplings, etc.) as well as conformational heterogeneity. However, general information could be obtained using chemical shift, isotope effect, dynamic NMR information as we have done previously (*1, 2*). For example, dynamic ^{19}F NMR spectra of FAAF modified Guanine (G_1) in *Nar*I 16mer sequence performed in our lab is shown below. Based on the chemical shifts at 5°C B, S, W conformations were assigned accordingly.

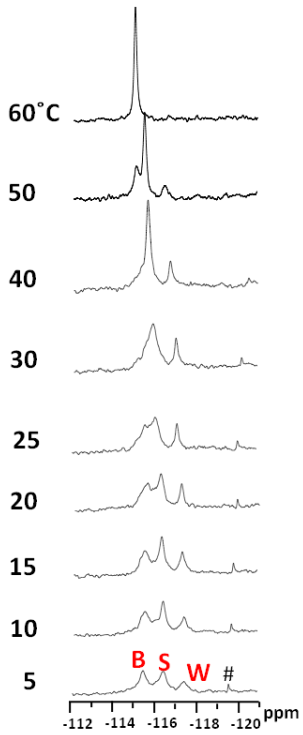

Circular Dichroism (CD) Spectroscopy

Circular Dichroism (CD) is a procedure that measures the ellipticities between the difference in the absorption of left and right handed circularly-polarized light. CD is sensitive to the changes occurring in chiral DNA and proteins. Chiral molecule characteristically produces a CD spectrum, depending on its spatial arrangement. Circular dichroism (CD) spectroscopy is a spectroscopic technique where the CD of molecules is measured over a range of wavelengths. CD spectroscopy is used extensively to study chiral molecules of all types and sizes. A primary use is in analyzing the secondary structure or conformation of macromolecules, particularly proteins as secondary structure is sensitive to its environment, temperature or pH, circular dichroism can be used to observe how secondary structure changes with environmental conditions or on interaction

with other molecules. Structural, kinetic and thermodynamic information about macromolecules can be derived from circular dichroism spectroscopy (*3*).

Measurements carried out in the visible and ultra-violet region of the electro-magnetic spectrum monitor electronic transitions, and, if the molecule under study contains chiral chromophores then one CPL state will be absorbed to a greater extent than the other and the CD signal over the corresponding wavelengths will be non-zero. A circular dichroism signal can be positive or negative, depending on whether left-handed circularly polarized light (L-CPL) is absorbed to a greater extent than R-CPL (CD signal positive) or to a lesser extent (CD signal negative). An example circular dichroism spectrum of a sample with multiple CD peaks is shown below, demonstrating how CD varies as a function of wavelength, and that a CD spectrum may exhibit both positive and negative peaks. It is an ideal by carcinogen and the presence of bulges and mismatches can be studied effectively by using this technique. Induced Circular Dichroism (ICD) is a novel technique and has been used for understanding interactions between chromophores and DNA and protein molecules. CD can be used to study the adduct-induced conformational heterogeneity, in the near-UV absorption range providing information about the binding nature of the carcinogen moiety. The CD measures ellipticities (deg*cm^2/dmol) as a function of wavelength (nm). Previously we carried out similar CD experiments in our lab on various carcinogens (AF and AAF modified duplexes), which gives us idea about the conformation of adduct-induced heterogeneity; disturbances such as distortion and disruption of Watson-Crick base pairs and bulge structures (*2*, *4*).

The figure shown below is a typical example for B-type DNA duplexes (Blue: unmodified; Red: Carcinogen modified) exhibiting CD ellipticity pattern characteristic

for a S-shape curve at around 275 (+) and 250 (-) nm, respectively. An increase in the positive intensity around 275nm in modified duplexes indicate an increase interaction of the modified base in the bulged pocket and a decreased positive intensity represents a decreased interaction of the carcinogen in the bulged pocket with the neighboring base pairs. Negative ellipticity at 290-320 nm is an indication of FAAF modification. In addition, adduct-induced shift (blue, short wavelength and red, longer wavelength) at 275nm indicate adduct induced DNA bending (*2*). The main advantage of CD is it requires less sample and the sample can be used again as the instrument does not destroy the sample unlike NMR, X-ray techniques but the main disadvantages are it produce excess noise when high concentration of buffers are used or when there is any particulate matter that interfere with CD signals. It cannot give detail information about the structures as NMR and X- ray (*5*).

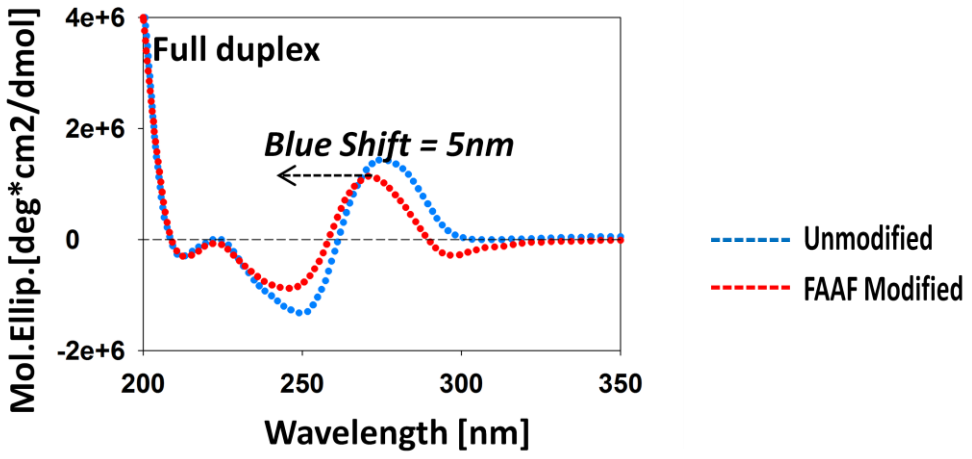

References:

1. Patnaik, S., and Cho, B. P. (2010) Structures of 2-acetylaminofluorene modified DNA revisited: insight into conformational heterogeneity, *Chem Res Toxicol 23*, 1650-1652.
2. Jain, V., Hilton, B., Patnaik, S., Zhou, Y., Chiarelli, M. P., and Cho, B. P. (2012) Conformational and thermodynamic properties modulate the nucleotide excision repair of 2-aminofluorene and 2-acetylaminofluorene dG adducts in the NarI sequence, *Nucleic Acids Res 40*, 3939-3951.
3. Greenfield, N., and Fasman, G. D. (1969) Computed circular dichroism spectra for the evaluation of protein conformation, *Biochemistry 8*, 4108-4116.
4. Jain, N., Li, Y., Zhang, L., Meneni, S. R., and Cho, B. P. (2007) Probing the sequence effects on NarI-induced -2 frameshift mutagenesis by dynamic 19F NMR, UV, and CD spectroscopy, *Biochemistry 46*, 13310-13321.
5. Bertucci, C., Pestalozzi, M., and De Simone, A. Circular dichroism in drug discovery and development: an abridged review, *Anal Bio anal Chem 398*, 155-166.

BIBILOGRAPHY

Ames, B. N., Gurney, E. G., Miller, J. A., and Bartsch, H. (1972) Carcinogens as frameshift mutagens: metabolites and derivatives of 2-acetylaminofluorene and other aromatic amine carcinogens, *Proc Natl Acad Sci U S A 69*, 3128-3132.

Belguise-Valladier, P., and Fuchs, R. P. P. (1991) *Biochemistry 30*, 10091

Beland, F. A., and Kadlubar, F. F. (1990) *Handbook of Experimental Pharmacology*, Spring-Verlag, Heidelberg.

Bresson, A., and Fuchs, R. P. (2002) Lesion bypass in yeast cells: Pol eta participates in a multi-DNA polymerase process, *EMBO J 21*, 3881-3887.

Chakrabarti, M. C., and Schwarz, F. P. (1999) Thermal stability of PNA/DNA and DNA/DNA duplexes by differential scanning calorimetry, *Nucleic Acids Res 27*, 4801-4806.

Cho, B. P., and Zhou, L. (1999) Probing the conformational heterogeneity of the acetylaminofluorene-modified 2'-deoxyguanosine and DNA by 19F NMR spectroscopy, *Biochemistry 38*, 7572-7583.

Cosman, M., Fiala, R., Hingerty, B. E., Amin, S., Geacintov, N. E., Broyde, S., and Patel, D. J. (1994) Solution conformation of the (+)-trans-anti-[BP]dG adduct opposite a deletion site in a DNA duplex: intercalation of the covalently attached benzo[a]pyrene into the helix with base displacement of the modified deoxyguanosine into the major groove, *Biochemistry 33*, 11507-11517.

Fuchs, R. P., Schwartz, N., and Daune, M. P. (1981) Hot spots of frameshift mutations induced by the ultimate carcinogen N-acetoxy-N-2-acetylaminofluorene, *Nature 294*, 657-659.

Fuchs, R. P., Koffel-Schwartz, N., Pelet, S., Janel-Bintz, R., Napolitano, R., Becherel, O. J., Broschard, T. H., Burnouf, D. Y., and Wagner, J. (2001) DNA polymerases II and V mediate respectively mutagenic (-2 frameshift) and error-free bypass of a single N-2-acetylaminofluorene adduct, *Biochem Soc Trans 29*, 191-195.

Fuchs, R. P., and Fujii, S. (2007) Translesion synthesis in Escherichia coli: lessons from the NarI mutation hot spot, *DNA Repair (Amst) 6*, 1032-1041.

Gao, L., Zhang, L., Cho, B., and Chiarelli, M. (2008) Sequence verification of oligonucleotides containing multiple arylamine modifications by enzymatic digestion and liquid chromatography mass spectrometry (LC/MS), *Journal of the American Society for Mass Spectrometry 19*, 1147-1155.

GD, F. (1996) *Circular Dichroism and the Conformational analysis of Biomolecules (Plenum press)*

Geacintov, N. E., Cosman, M., Hingerty, B. E., Amin, S., Broyde, S., and Patel, D. J. (1997) NMR solution structures of stereoisometric covalent polycyclic aromatic carcinogen-DNA adduct: principles, patterns, and diversity, *Chem Res Toxicol 10*, 111-146.

Heflich, R. H., and Neft, R. E. (1994) Genetic toxicity of 2-acetylaminofluorene, 2-aminofluorene and some of their metabolites and model metabolites, *Mutation Research/Reviews in Genetic Toxicology 318*, 73-174.

Hoffmann, G. R., and Fuchs, R. P. P. (1997) Mechanisms of Frameshift Mutations:â€‰ Insight from Aromatic Amines, *Chemical Research in Toxicology 10*, 347-359.

Hsu, G. W., Kiefer, J. R., Burnouf, D., Becherel, O. J., Fuchs, R. P. P., and Beese, L. S. (2004) Observing Translesion Synthesis of an Aromatic Amine DNA Adduct by a High-fidelity DNA Polymerase, *J. Biol. Chem. 279*, 50280-50285.

Jain, N., Li, Y., Zhang, L., Meneni, S. R., and Cho, B. P. (2007) Probing the sequence effects on NarI-induced -2 frameshift mutagenesis by dynamic 19F NMR, UV, and CD spectroscopy, *Biochemistry 46*, 13310-13321.

Jain, N., Meneni, S., Jain, V., and Cho, B. P. (2009) Influence of flanking sequence context on the conformational flexibility of aminofluorene-modified dG adduct in dA mismatch DNA duplexes, *Nucleic Acids Res 37*, 1628-1637.

Jain, V., Hilton, B., Patnaik, S., Zou, Y., Chiarelli, M. P., and Cho, B. P. Conformational and thermodynamic properties modulate the nucleotide excision repair of 2-aminofluorene and 2-acetylaminofluorene dG adducts in the NarI sequence, *Nucleic Acids Res 40*, 3939-3951.

Koffel-Schwartz, N., and Fuchs, R. P. (1995) Sequence determinants for -2 frameshift mutagenesis at NarI-derived hot spots, *J Mol Biol 252*, 507-513.

Koffel-Schwartz, N., Verdier, J. M., Bichara, M., Freund, A. M., Daune, M. P., and Fuchs, R. P. (1984) Carcinogen-induced mutation spectrum in wild-type, uvrA and umuC strains of Escherichia coli. Strain specificity and mutation-prone sequences, *J Mol Biol 177*, 33-51.

Liang, F., and Cho, B. P. (2010) Enthalpy-entropy contribution to carcinogen-induced DNA conformational heterogeneity, *Biochemistry 49*, 259-266

Luch, A. (2005) Nature and nurture - lessons from chemical carcinogenesis, *Nat Rev Cancer 5*, 113-125.

Mao, B., Cosman, M., Hingerty, B. E., Broyde, S., and Patel, D. J. (1995) Solution conformation of [AF]dG opposite a -1 deletion site in a DNA duplex: intercalation of the covalently attached aminofluorene ring into the helix with base displacement of the C8-modified Syn guanine into the major groove, *Biochemistry 34*, 6226-6238.

Mao, B., Gorin, A., Gu, Z., Hingerty, B. E., Broyde, S., and Patel, D. J. (1997) Solution structure of the aminofluorene-intercalated conformer of the syn [AF]-C8-dG adduct opposite a--2 deletion site in the NarI hot spot sequence context, *Biochemistry 36*, 14479-14490.

Meneni, S. R., D'Mello, R., Norigian, G., Baker, G., Gao, L., Chiarelli, M. P., and Cho, B. P. (2006) Sequence effects of aminofluorene-modified DNA duplexes: thermodynamic and circular dichroism properties, *Nucleic Acids Res 34*, 755-763.

Meneni, S. R., Shell, S. M., Gao, L., Jurecka, P., Lee, W., Sponer, J., Zou, Y., Chiarelli, M. P., and Cho, B. P. (2007) *Biochemistry 46*, 11263.

Milhe, C., Dhalluin, C., Fuchs, R. P., and Lefevre, J. F. (1994) NMR evidence of the stabilisation by the carcinogen N-2-acetylaminofluorene of a frameshift mutagenesis intermediate, *Nucleic Acids Res 22*, 4646-4652

Milhe, C., Fuchs, R. P., and Lefevre, J. F. (1996) NMR data show that the carcinogen N-2-acetylaminofluorene stabilises an intermediate of -2 frameshift mutagenesis in a region of high mutation frequency, *Eur J Biochem 235*, 120-127.

O'Handley, S. F., Sanford, D. G., Xu, R., Lester, C. C., Hingerty, B. E., Broyde, S., and Krugh, T. R. (1993) Structural characterization of an N-acetyl-2-aminofluorene (AAF) modified DNA oligomer by NMR, energy minimization, and molecular dynamics, *Biochemistry 32*, 2481-2497.

Ohmori, H., Friedberg, E. C., Fuchs, R. P., Goodman, M. F., Hanaoka, F., Hinkle, D., Kunkel, T. A., Lawrence, C. W., Livneh, Z., Nohmi, T., Prakash, L., Prakash, S., Todo, T., Walker, G. C., Wang, Z., and Woodgate, R. (2001) The Y-family of DNA polymerases, *Mol Cell 8*, 7-8.

Patnaik, S., and Cho, B. P. (2010) Structures of 2-acetylaminofluorene modified DNA revisited: insight into conformational heterogeneity, *Chem Res Toxicol 23*, 1650-1652

Roy, D., Hingerty, B. E., Shapiro, R., and Broyde, S. (1998) A slipped replication intermediate model is stabilized by the syn orientation of N-2-aminofluorene- and N-2-(acetyl)aminofluorene-modified guanine at a mutational hotspot, *Chem Res Toxicol 11*, 1301-1311.

Schaaper, R. M., Koffel-Schwartz, N., and Fuchs, R. P. P. (1990) N-acetoxy-N-acetyl-2-aminofluorene-induced mutagenesis in the lacI gene of Escherichia coli., *Carcinogenesis 11*, 1087.

Schorr, S., and Carell, T. (2010) Mechanism of acetylaminofluorene-dG induced frameshifting by polymerase eta, *Chembiochem 11*, 2534-2537.

Shibutani, S., Suzuki, N., Tan, X., Johnson, F., and Grollman, A. P. (2001) Influence of Flanking Sequence Context on the Mutagenicity of Acetylaminofluorene-Derived DNA Adducts in Mammalian Cells, *Biochemistry 40*, 3717-3722.
Shibutani, S., Suzuki, N., Tan, X., Johnson, F., and Grollman, A. P. (2001) Influence of Flanking Sequence Context on the Mutagenicity of Acetylaminofluorene-Derived DNA Adducts in Mammalian Cells, *Biochemistry 40*, 3717-3722.

Suzuki, N., Yasui, M., Santosh Laxmi, Y. R., Ohmori, H., Hanaoka, F., and Shibutani, S. (2004) Translesion synthesis past equine estrogen-derived 2'-deoxycytidine DNA adducts by human DNA polymerases eta and kappa, *Biochemistry 43*, 11312-11320.

Zhang, Y., Yuan, F., Wu, X., Rechkoblit, O., Taylor, J. S., Geacintov, N. E., and Wang, Z. (2000) Error-prone lesion bypass by human DNA polymerase eta, *Nucleic Acids Res 28*, 4717-4724.

Zhou, L., Rajabzadeh, M., Traficante, D. D., and Cho, B. P. (1997) Conformational Heterogeneity of Arylamine-Modified DNA: 19F NMR Evidence, *J Am Chem Soc 119*, 5384-5389